

UTRECHT UNIVERSITY



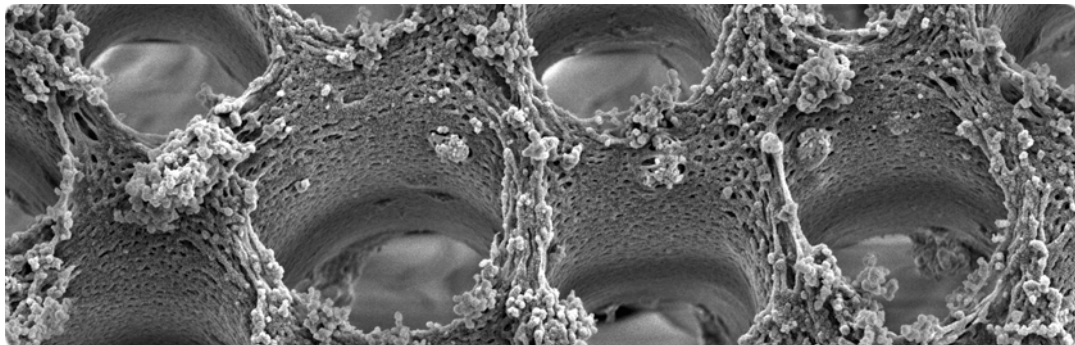
NATURAL SCIENCE THESIS

Feasibility of Phase Immersion Precipitation for the Application of Electrode Production: A Literature & Parameter study.

"A chain is no stronger than its weakest link"

Author:
L N STURKENBOOM BSc

Supervisors:
T VAN DIJK MSc
B VAN DEN BOSCH PhD
Prof. Dr. F MULDER
Prof. Dr. Ir. E ROESINK



*A thesis submitted in fulfilment of the requirements
for the degree of MSc Energy Science*

in the

Faculty of Geosciences

and as supportment for the development

of

E-Stone Batteries



March 2015

UTRECHT UNIVERSITY

Abstract

Faculty of Geosciences

MSc Energy Science

Feasibility of Phase Immersion Precipitation for the application of electrode production.

by L N STURKENBOOM

To attain high accessible amounts of active material in electrodes of aqueous batteries, this thesis investigates the possibility to create porous structures by introducing a simple low-cost production method for polymeric supports solidifying active material, without applying heat nor pressure. This technique is based on phase inversion activated by liquid/liquid or gas/liquid demixing. The polymerbinder used for this technique has to be resistant to chemicals, temperature- and volume changes occurring on and in the anode and yet be highly miscible in solutes to be used for phase inversion techniques as well. As a case study common used polymers, Polyvinylidene Fluoride and Polyethersulfone, and common used enhancement techniques for the production of synthetic membrane filters have been applied to create Iron Sulphide anodes. SEM and porosity analysis show that films produced by phase immersion precipitation do solidify Iron Sulphide and an open homogeneous microporous structure can be obtained with cross-section pore sizes ranging from 0,1-10 μm and surface pores ranging from 0,5-6 μm with a pore volume of 60 %. In comparison pore sizes ranging from 0,1-0,5 μm with a pore volume of 50 % results by using conventional pressed electrodes. Caution needs to be taken for to highly porous structures and to high amounts of insulating polymer binder as well, as both could negatively affect electronic conductivity. As a proof of principal cycling experiments of anodes produced by this novel production method for a Nickel-Iron Sulphide battery show capacities of 180 mAh/g for more than 55 cycles with an average Charge/discharge efficiency of 82 % can be obtained, by cycling between Fe(II)/Fe(III) only, to prevent the hydrogen evolution. The achievement of interesting porous structures and increase in porosity compared to conventional production techniques combined with promising cycling results suggest PI by liquid/liquid and gas/liquid demixing techniques could be an interesting production technique.

Acknowledgements

I am still astonished of what is possible in half a year.

Thank you Thomas, Vera, Bram, Bob, Bart, Thomas, Dennis, Fokko, Erik and Raymond for the relaxed working environment and extra hands. . .

Contents

1	Introduction	1
1.1	From human affected- to environmental dependence	1
1.2	The last shall be first, and the first last	2
1.3	Combining expertise	4
2	Phase Immersion Precipitation	6
2.1	Description of technique	8
2.2	Selecting the right binder for PI produced FeS anodes: PVDF vs. PES . .	13
2.2.1	PVDF	15
2.2.2	PES	17
3	Porosity enhancement methods for PVDF	20
3.1	Experimental section	20
3.2	Results & discussion	21
3.3	Conclusion	24
4	Porous membranes as FeS electrode support	25
4.1	Experimental section	25
4.2	Results & discussion	26
4.2.1	SEM cross-sections of PIP membranes compared	26
4.2.2	SEM cross-sections of IPV membranes compared	28
4.2.3	SEM surface imagery of membranes & pressed pills compared . . .	29
4.2.4	Pore space analysis of PIP & IPV membranes & pressed pills compared	31
4.3	Conclusion	32
5	Cycling performance of PIP and IPV produced FeS anodes	33
5.1	Experimental section	34
5.2	Results & discussion	35
5.2.1	PES versus PVDF & PIP versus IPV	35
5.2.2	PVDF with 15 wt% conductive additive	37
5.2.3	PVDF with conductive additive super p	39
5.2.4	Ballmilling	40
5.3	Conclusion	41
6	Conclusion	42
7	Discussion	44

A Polymer synthesis, morphology and properties	47
B 200 °C oven treatment	56
C SEM photos of FeS, Super P & PVDF particles	57
D Results of a pure pressed FeS anode	59
Bibliography	60

List of Figures

1.1	Ragone plot with envisaged performance of a commercial NiFeS battery; E-Stone, T. van dijk (2014)[1]	3
2.1	Scanning Electronic Microscope (SEM) surface images of polymeric microfiltration membranes: a) By PIP, b) by thermal precipitation, c) by track etching and d) by stretching, E. Roesink (1989) [2]	7
2.2	schematic representation of a) PIP or b) IPV. The polymer solution consists of a polymer:solvent. J_{in} is the non-solvent flux into the solution and J_{out} the solvent flux out the solution in the coagulation bath.	9
2.3	SEM cross-sections of a Polyetherimide (PEI) membrane obtained by: a) direct PIP. (take note of the macrovoids, almost as large as the film.) b) 5 min. IPV and PIP afterwards. c) PIP containing solvent:non-solvent = 90:10 wt%, E. Roesink (1989)[2]	9
2.4	Two schematic ternary diagrams. In a) three different pathways are shown through the Nucleation and Growth (NG) area, indicated between the binodal and spinodal line and following the Spinodal Decomposition (SD) area. Pathway A only results in a porous structure, C. Barth et al. (2000)[3]. b) shows a typical pathway through the different phases of the system, L. Vogelaar et al. (2005).[4]	10
2.5	calculated initial composition paths in PIP for CA/dioxin/water system with varying initial volume fractions, J. Mulder (1996).[5]	11
2.6	Schematic ternary diagrams with calculated composition paths for: a) CA/dioxin/water system with varying initial volume fractions, b) for the system CA/dioxin/water with different fractions of dioxin in the CB & c) for the system CA/acetone/water with varying non-solvent content in initial solution, J. Mulder (1996)[5]	13
2.7	SEM cross sections of membranes by PIP with the system PVDF/solvent/water having solvents: a) TEP, b) NMP, c) DMF and d) DMAc. Higher solubility of PVDF in the solvent increases porous structure of the resulting membrane, K. Wang (1989).[6]	15
2.8	SEM crosssections of membranes by PIP with the system PVDF/DMF/non-solvent having non-solvent: a) water and b) ethanol. Higher affinity between solvent/non-solvent increases porous structure, K. Wang (1989)[6]	16
2.9	SEM cross sections of membranes prepared by the system PES 49w/DMF/H ₂ O, C. Barth (2000).[3]	18
2.10	Ternary diagram showing the binodal for the system a) PVDF/NMP/non-solvent for different non-solvents, K. Wang (1999) and b) PES/solvent/water for different solvents, W. Lau (1991).[6, 7]	18

3.1	Thickness and density for different initial concentrations PVDF:NMP (wt%) for PIP- & IPV membranes, respectively shown above and below. The different coloured plots indicate the temperature of CB used. The black PVDF plots show the calculated thickness and density of membranes following the PVDF:NMP concentration of the solution.	22
3.2	Thickness and density for different initial concentrations PVDF:NMP(wt%) when adding 10 wt% solvent to the CB and the use of DMSO is compared to NMP. The black PVDF plot shows the thickness and density following the PVDF:NMP concentration of the solution. CB & VT means respectively PIP and IPV.	23
3.3	Breaking stress for PIP and IPV at different initial concentrations PVDF:NMP (wt%).	23
4.1	Above SEM cross-sections and below an enlargements of PIP membranes are shown by the system a) FeS/PVDF/NMP/H ₂ O, 25 % FeS/PES. b) FeS/PES/NMP/H ₂ O, 25 % FeS/PES. c) FeS/PES/NMP/H ₂ O, 50 % FeS/PES. For all preceding, the initial concentration is 20 % PES/solvent. d) FeS/Super P/PES/90 % DMSO/10 % acetone/H ₂ O 80 % FeS/15 % Super P/PES, Initial concentration is 10 % PES/solvent.	27
4.2	SEM cross sections of IPV films produced by the system a) FeS/PVDF/DMSO/H ₂ O resulting in the laminate 95 % FeS/PES, b) FeS/PES/DMSO/H ₂ O resulting in 95 % FeS/PES and c) FeS/PES/NMP/H ₂ O resulting in 95 % FeS/PES. The figures below show enlargements of the above.	28
4.3	SEM toplayer surface imagery of membranes. PIP, 25 wt% FeS/PVDF/NMP/H ₂ O. PIP, 50 wt% FeS/PES/NMP/H ₂ O, shows the bottom layer. Junction, 50 wt%FeS/PES/NMP/H ₂ O. IPV and PIP are made by the same system 95 wt% FeS/PES. The pressed pill contains FeS/Super P/PVDF in the ratio 82:10:8 wt%	30
5.1	A typical charge discharge plot of a NiFeS battery with its corresponding plateau's shown, Van Dijk (2012).[8]	34
5.2	Activation cycles followed by Fe(II)/Fe(III) cycling, Van Dijk (2012).[8]	34
5.3	For FeS/PES versus FeS/PVDF, capacities in mAh/g plotted against the no. of cycles and below for cell 17 and 21 the voltage plotted against the time. Also as an example, for cell 47 the theoretical depletion of electrolyte is shown versus the time. CB means direct PIP and VT means IPV.	36
5.4	For FeS/PVDF with 15 wt% conductive additives, capacities in mAh/g and efficiencies plotted against the no. of cycles. below for cell 15 and 10 the voltage is plotted against the time. The progress in cycling is indicated by a color change from blue to red. For cycle 11 and 31 the capacity against the voltage plots are compared for anodes containing Graphite, SP and no additive. VT means IPV.	38
5.5	For FeS/PVDF with increasing SP additive capacities in mAh/g and efficiency plotted against the no. of cycles and below for cell 12 and 16 and 40 the voltage plotted against the time. The progress in cycling is indicated by a color change from blue to red. Also a total voltage plot versus the time for cell 40 is shown below. CB and VT respectively means PIP and IPV.	40

5.6	The voltage plotted against the time for balmilled and not balmilled active material. CB means direct PIP and VT means IPV.	41
A.1	Polymer structuring possibilities	48
A.2	Polymer structuring possibilities	48
A.3	flexible and rigid polymer chains	49
A.4	polymer chains with an enlargement of an interaction site	50
A.5	Type of crystallites	51
A.6	Tensile modulus of a polymer as a function of the temperature. a)crystalline polymer; b)semi-crystalline polymer; c)amorphous polymer.	52
A.7	Polymer blends	53
B.1	Thickness decrease and density increase due to 200 °C oven treatment of a 0,5 mm casted a) PIP & b) IVP membrane.. . . .	56
C.1	SEM photos of balmilled FeS, Super P and PVDF	57
D.1	efficiency and capacity plot versus the no. of cycles, voltage plot versus the time and voltage versus capacity	59

List of Tables

1.1	Performance parameters compared to envisaged NiFeS for stationary storage , T. van dijk (2014) [1]	2
2.1	Properties of production methods for filtermembranes.[5]	6
2.2	PI techniques and their system, the occurring process and the resulting membrane obtained by the process.[2, 5, 9]	8
2.3	Properties of PVDF and PES	19
3.1	An estimation of pore volume using different enhancement techniques looking to Δt & Δq	24
4.1	Density analysis.	31
A.1	relation between molecular weight of a polymer and its resulting character	47
A.2	Proton donor and -acceptor character of most common groups	51
A.3	Classification of solvent/non-solvent pairs	54
A.4	General characteristics of common used microfiltration polymers	55
C.1	Spot elementary Analysis	58

Abbreviations

BET	B runauer E mmet T eller
BS	B reaking S tress
CA	C yano A cetate
DMAc	D i M ethyl A cetamide
DMF	D i M ethyl F ormamide
DMSO	D i M ethyl S ulf O xide
Fe	I ron
Fe₂O₃	F erric oxide
Fe(OH)₂	F errous I ron
HER	H ydrogen E volution R eaction
HMPA	H exa M ethyl P hospor A mide
IPV	I mmersion P recipitation from the V apour phase
KOH	P ottasium hydroxide
NG	N ucleation & G rowth
NiFe	N ickel I ron
NiFeS	N ickel I ron S ulphide
NMP	N - M ethyl-2- P yrrolidone
PAN	P oly A crylon N itrile
PE	P oly E thylene
PEG	P oly E thylene G lycol
PES	P oly E ther S ulfone
PI	P hase I nversion
PIP	P hase I mmersion P recipitation
Plu	P luronic
PMMA	P oly M ethyl M eth A crylate

PP	P oly P ropylene
PS	P oly S ulfone
PV	P ore V olume
PVDF	P oly V inyl D ene F luoride
PVP	P oly V inyl P yrrolidone
PTFE	P oly T etra F luor E thylene
P-TFE-VDF	P oly- T etra F luor E thylene- V inyl D ene F luoride
SD	S pinodal D ecomposition
SEM	S canning E lectronic M icrograph
TEP	T ri E thyl P hosphate

To Linda...

Chapter 1

Introduction

1.1 From human affected- to environmental dependence

Energy storage systems

Production of renewable energy conversion technologies and their resource are directly intertwined. The actual yield is dependent of the occurrence of the renewable such as the sun or wind. In comparison with conventional fuels used today, energy production cannot be regulated. Hence a large-scale transition to a renewable energy economy will cause daily and seasonal intermittent and intrinsically variable generated electricity at moments it is not required directly, such as F. M. Mulder (2014) recently depicted. [10, 11]

Stationary energy storage systems could enable to cope with overproduction but no single storage system today meets all requirements-e.g.: Mature technology, long lifetime, robust, low-cost, abundant materials, high efficiency and being environmentally benign. As a consequence, renewable energy technologies are not yet implementable on a large-scale to be cost-competitive with conventional methods.[11–13] Moreover, improved storage systems could also diminish the demand for fluctuating energy production. As it provides the opportunity to implement more conventional cheap production methods for variable load, such as nuclear energy.[13]

Electrochemical storage systems

Hence storage systems are urgently required to be improved. Interesting options on the short-term are hydro-, heat- and electrochemical storage.[11, 13] Hydro-storage depends on geographical factors, thus is limited in scale and has degrading effects for ecological zones.[11] Storage in the form of heat is most efficient in combination with a direct heat

source such as concentrated solar plants, but still the rather low efficiencies are seen as a limiting factor. Electrochemical storage in the form of batteries is the oldest form of energy storage and seem ideally suited for electrical storage applications. Batteries provide fuel flexibility, environmental- and operating benefits to electricity utility.[13]

Still batteries are not implemented on a large scale for stationary energy storage due to their low energy- and capacity densities, high maintenance costs, too short cycle lives, limited discharge capabilities or utilization of rare and toxic materials.[13] Following recent literature, batteries that are either in use or most suitable for stationary battery energy storage applications include lithium-ion, lead-acid, nickel-cadmium, sodium-sulphur and sodium-nickel-chloride, without mentioning Nickel-Iron-Sulphide (NiFeS).[11–14]

1.2 The last shall be first, and the first last

The Nickel Iron battery

In 1901 Edison introduced one of the first batteries ever made: The Nickel-Iron (NiFe) battery. This battery already had an impressive performance of 3000 cycles with an energy efficiency of 80-65% resulting in a cycle life ranging from 20-50 years.[15] Nonetheless, its low specific energy of around 30-50 Wh/kg in combination with self-discharge by corrosion and high costs of manufacture of the Fe electrode resulted the NiFe battery to be outcompeted by other types, such as nickel-cadmium and lead-acid.[8, 15, 16]

TABLE 1.1: Performance parameters compared to envisaged NiFeS for stationary storage, T. van dijk (2014) [1]

	Li	Pb	NiCd	NiMH	NiFeS
Lifetime	+	--	++	++	+++
Production Costs	-	++	+	+-	+
Production Process	-	++	+	+-	+
Environmental Hazards	-	-	--	-	+
Recycling	-	+	-	-	++
Availability	-	+	-	-	++
Efficiency	+++	-	-	+	+

Today, probably lead-acid batteries dominate the off-grid energy market because of the maturity of the technology that resulted in cheap production costs, availability of the materials used and its maintenance free character. Though, the lifetime of the acid is 3-4 years, which is far too short.[8] Lithium-ion based batteries show best performances and the technology is innovating quickly in the recent years. Unfortunately, actual large scale implementation for stationary purposes is limited due to the high costs of special packaging and the low natural occurrence of Lithium.[13, 17] In table 1.1 envisaged performance parameters of NiFeS are compared to those of other battery types.[1]

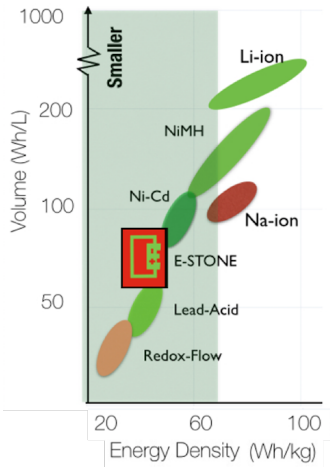
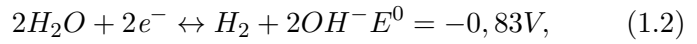


FIGURE 1.1: Ragone plot with envisaged performance of a commercial NiFeS battery; E-Stone, T. van dijk (2014)[1]

The last decade there has been renewed interest in Ni-Fe batteries due to their superiority in robustness and the utilization of non-toxic, environmentally benign and cheap materials.[8, 15] Nonetheless, still same cutbacks arise Edison had to deal with back in 1901. The low charging efficiency is due to the Hydrogen Evolution Reaction (HER) that takes place between the Fe electrode and the aqueous potassium hydroxide (KOH) electrolyte. Under alkaline conditions the standard reduction potential of the water/hydrogen couple is close to the ferrous-/metallic iron couple,



which causes a parasitic effect, leading to the decomposition of the aqueous electrolyte into hydrogen gas. As a consequence a loss of charging current occurs and the overall coulombic efficiency declines. Besides, the eventual rate capabilities are poor due to the passivation of Fe in the anode. Upon discharge electrically insulating ferrous iron ($Fe(OH)_2$) is formed, which results into a decrease in cell voltage.[8, 15] Increasing the efficiency and rate capability are prerequisites for the NiFe battery to be an interesting candidate for stationary energy storage.

Addition of Sulphides to Iron electrodes

Recent studies show that sulphur or bismuth containing additives at the Fe anode have a strong influence on the cycling efficiency and the discharge performance.[10, 18–23]. T. van Dijk (2012) founder of E-Stone Batteries, managed to retrieve more than 150 cycles in two months with an energy efficiency of 82% by using NiFeS and by only cycling between Fe(II)/Fe(III). This resulted in capacities of 330 W/kg and 120 Wh/kg, which is a doubling compared to commercial NiFe batteries available today.[8] A comparison in densities to other battery types is given in figure 1.1.[8] Sulphides have proven to mitigate passivation and help sustain high discharge rates at the Fe electrode. Nonetheless the role of these additives for electrode passivation and inhibition of the HER have not yet been fully understood and further research by E-Stone Batteries and others proved reproducibility is a common issue.[10, 18–23]

Increase ionic conductivity while lowering production costs

E-Stone Batteries is aware of the necessity of a thorough parameter study to maintain reproducibility. Porosity of the electrode is such a critical performance parameter of a battery influencing ionic conductivity, which T. van Dijk has not yet investigated. The anode is traditionally sintered but by doing so unwanted reactions can be initiated and the structure of the material can change. T. van Dijk achieved the results mentioned above by dry pressing pure FeS. Together with sintering anodes little attention is given to produce a high surface reactivity.[8] When a polymer is used as binder solidifying the electrode, another often underestimated parameter is the influence of the properties of the polymer for the electronic- and ionic conductivity of an electrode. In electrochemical literature the influence of a binder for the overall performance of a battery is stressed, such as Kitamura et al. (2012) does for NiFe batteries.[24–26] The limiting factor of reproducibility together with finding ways to lower production costs and increase the performance of the anode resulted in collaboration between E-Stone Batteries and Prof. E Roesink of the University of Twente. Both parties found two interesting fields of study to combine: Phase Immersion Precipitation (PIP) for the production of electrodes.

1.3 Combining expertise

Phase Immersion Precipitation

PIP is studied intensively in membrane science to create polymeric nano- and microfiltration membranes. Next to its simplicity, PIP enables to achieve precise pore sizes and certain structures to influence the permeability of a filter, for particles, gas or liquid. Next to porosity PIP can also influence other parameters as hydrophobicity, ionization and catalysis.[2, 5] For electrochemical applications we focus on highly inert polymers and methods to produce liquid microfiltration membranes for the creation of a synthetic support for active material, in this case FeS.

Ideal porous morphology of electrodes

Depicted on the front cover of this thesis is an example of a theoretical model of an ideal porous morphology for electrodes, as proposed by prof F. M. Mulder of the faculty of chemical engineering at TU Delft and chief scientist at E-Stone Batteries. The structure consists out of evenly distributed tubular-like pores, acting as highways for the ions in aquatic solution, with smaller pores surrounding these highways. In theory the tubular-like pores than favour electrolyte permittivity while the smaller pores benefit the surface reactivity of the active material. Both pore sizes must not be too big nor too small. The former decreases electronic- while the latter decreases ionic conductivity, or an

electronic conducting foam must be applied instead. Hence a trade-off can be found. PIP membranes are characterized by the possibility to create fingerlike porous structures with smaller pores surrounding these, similar to the structure proposed.[5]

PIP for the production of low-cost porous electrodes

Comparable Phase Inversion (PI) induced production techniques exist in the electrochemical industry with a polymer functioning as binder to solidify all components of the electrode-e.g. drying and sintering. Then most attention is given to which polymer and technique gives best strength for solidifying the electrode.[8] PIP is used as a way of producing solid and selective separators, indicated by Zhang (2007) or more specific by Magistris et al. (2000) and A Du Pasquier (2002).[27–29] PIP is also recently studied by for example Jin et al. (2010) and Zhao et al. (2011) for the production of anode supports for solid oxide fuel cells.[30, 31]. In contrast little academic- or commercial research is done for the possibility of PIP electrode production, following a thorough literature and patent study. This is surprising considering the resemblance; to other production techniques mentioned and in electrochemistry of fuel cells, while having apparent advantages in ease of production, resulting thickness and porosity.[32]

Aim of this study, hypothesis & approach

This study aims to give more insight in which type of polymer-binder is interesting to use for the anode E-Stone Batteries develops and explores the feasibility of PIP as a ways of production for anodes. Hence the research question is:

Which kind of polymer-binder fits best in a FeS electrode of a NiFeS battery?

With the sub-question:

Is phase immersion precipitation a feasible production technique?

By applying PIP techniques the main goal is to enhance the accessibility of active material by positively affecting the ionic conductivity in the FeS anode. As PIP could enable to decrease the thickness and increase the porosity. Parameters of the electrode that must not be delimited by doing so are the rigidity, electronic conductivity, endurance and reproducibility. Hence the properties of the polymer need to be investigated as well.

In Chapter 2 PI techniques and polymers are explained that are most suitable for porous structures in a NiFeS battery. Chapter 3 shows a simple first experiment to acquaint the technique and achievement of porous structures for pure polymer laminates. Following Chapter 4 gives more insight in the achievement of porous structures for polymer supports solidifying the active material, following a SEM and pycnometry analysis. In Chapter 5 than PIP produced anodes are tested in actual battery cycling, followed by an overall conclusion and discussion in respectively Chapter 6 and 7.

Chapter 2

Phase Immersion Precipitation

PIP is part of the PI family. PI of polymer solutions is most widely used to create synthetic membranes for micro- and ultrafiltration separation purposes, defined respectively as 0,1-10 μm , and 2-100 nm. Other ways to prepare porous polymeric membranes are shown in table & figure 2.1. Apart from its superiority in simplicity, PI distinguishes itself by the possibility to produce different types of interesting porous structures, to precisely create and obtain a wide range of sizes, to be able to alter the availability of pores and to obtain other wanted characteristics, such as separation based on hydrophobicity, ionization and catalyses.[2, 5, 9] The achievement of these features depends respectively on a variety of technique procedures. Main difficulty using PIP is the lack of a predictable and systematic method.[6] The resulting structure also seems to follow the characteristics of the polymers used. In fact the thermal, chemical and mechanical properties of a certain polymer are decisive for the applicability for PIP and what type of porous structures can be achieved. Therefore the development of highly resistant membranes comes with the introduction of new engineering plastics, such as Ultem[®] polyetherimide, Victrex[®] polyetherketone, Noryl[®] polyphenyleneoxide and Ultrason[®] PolyEtherSulfone (PES).[2]

TABLE 2.1: Properties of production methods for filtermembranes.[5]

Method	Polymer	Poresize (μm)	Achievable porosity	Applied for electrode production
Sintering	Wide	0,1-10	Low (15 %)	Common
Stretching	(Semi)Crystalline	0,1-3	high (90 %)	-
Track-etching	Wide	0,02-10	Low (10 %)	-
Template leaching	Glassy polymer	Wide	Low-high	-
Phase Inversion	Solvable polymer	Wide	Low-high	Little

Thus before further elaborating on the technique it is recommended to refresh our memories with the basics of polymer chemistry. In *Appendix A* a diverted summary is given of "The Basic Principles of Membranes" by Jan Mulder (1996): Chapter 2, "Materials and material properties". Also an overview is given of polymer-groups and their characteristics, which polymers are applicable for which technique and which polymers are used to create porous or dense structures. When you might already have a thought of how the basics work, please do not hesitate to continue reading. First a description of the technique is given and its parameters influencing porosity. Following two polymers are compared, seeming to be best applicable for the FeS anode, E-Stone Batteries researches: PolyVinylidene Fluoride (PVDF) and PolyEtherSulfone (PES).

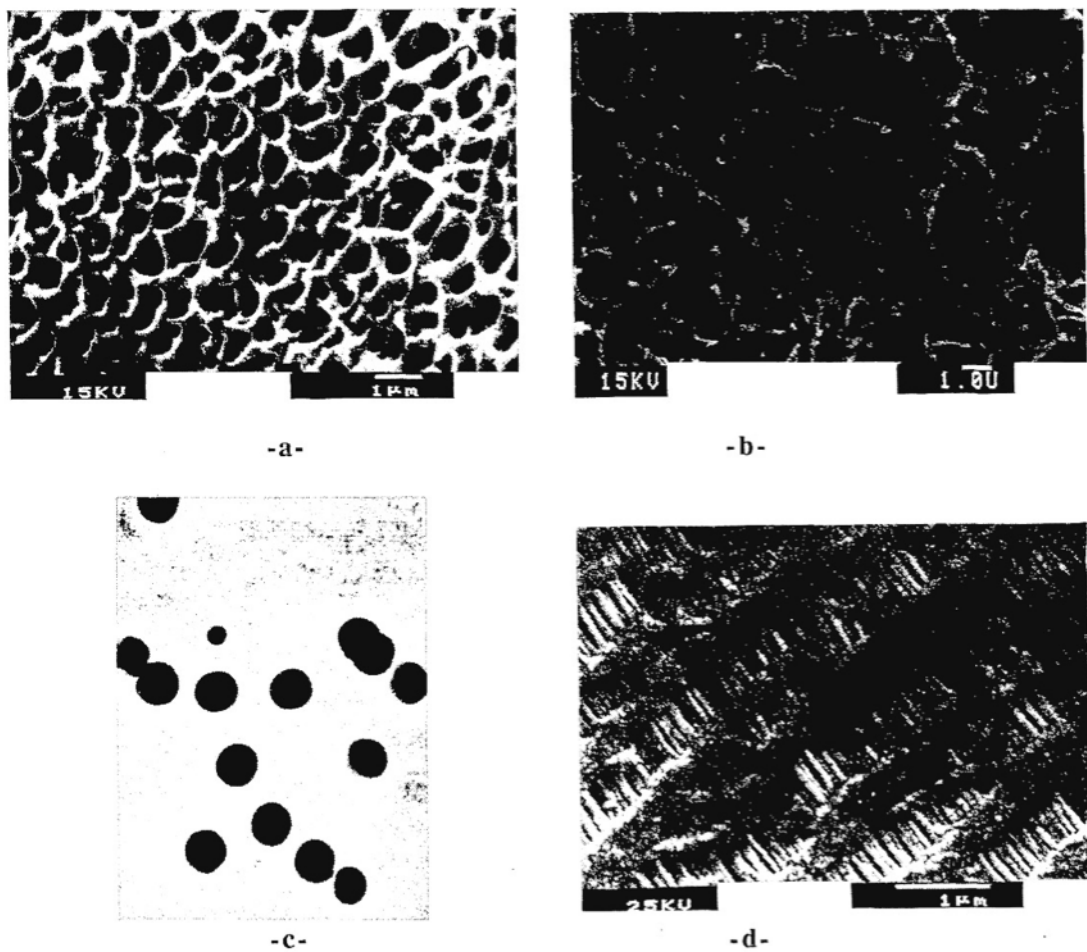


FIGURE 2.1: Scanning Electronic Microscope (SEM) surface images of polymeric microfiltration membranes: a) By PIP, b) by thermal precipitation, c) by track etching and d) by stretching, E. Roesink (1989) [2]

2.1 Description of technique

Phase Inversion

PI begins with a polymer dissolved in its solvent that can be casted, moulded, coated or injected in a certain wanted configuration. When adding the non-solvent, not solvable for the polymer but solvable for the solvent, a two-phase separation occurs in a polymer poor phase filling the pores and a polymer rich phase forming a continuous membrane matrix. The PI is triggered by a thermodynamical instability either by a change in composition or a change in temperature of the polymer solution. PS techniques can be separated by different systems shown in table 2.2. Figure 2.3 shows cross-sections of the actual pores obtained by different techniques. To achieve porous structures, mostly l/l- and l/g PI demixing techniques are used. These are also most commercially used. Mostly structure-related properties such as pore size, pore size distribution, top layer thickness and surface porosity determine the actual permeation in the micro-range. In the ultra-/nano range also chemical properties between the polymer and solute come into play, such as adsorption and hydrophilic characteristics.[2, 5, 9]

TABLE 2.2: PI techniques and their system, the occurring process and the resulting membrane obtained by the process.[2, 5, 9]

Method	solvent:non-solvent	Activating process	Membrane obtained
Solvent evaporation	l/g	Evaporation solvent	Dense homogeneous nano for gas separation
Controlled evaporation	l/g	Volatility of solvent leads to precipitation	Skinned (layered)
Thermal induced	l/l	ΔT influences miscible behaviour solvent	Skinned micro
<i>Phase Immersion Precipitation (PIP)</i>	l/l	Mass transfer	Micro-macro with dense top layer for g/l separation
<i>Precipitation from the vapour phase (IPV)</i>	l/g	J_{in} non-solvent	Micro-meso pores without dense top layer for g/l separation

Phase immersion precipitation

PIP membranes are produced by casting or moulding a polymer solution consisting of a polymer and a solvent as a thin film on a support, shown in figure 2.2a. Following, the thin film on its support is directly submerged in a Coagulation Bath (CB) containing the non-solvent. This results in an exchange: indiffusion of non-solvent (J_{in}) and outdiffusion of solvent (J_{out}). What follows is a thermodynamic instability in the thin film solution, resulting in demixing and aggregate formation, and following precipitation of the polymer. By PIP the typical asymmetric fingerlike porous structure can be obtained. In principal, instantaneous demixing favours faster precipitation, thereby less membrane

shrinkage occurs and consequently a creation of a more porous structure, shown in figure 2.7a. The shrinkage is also the reason the film gets loose from its support. On the contrary, delayed onset of the demixing favours a more dense structure, shown in figure 2.7b. During faster instantaneous demixing, the concentrations of the outdiffusion of the solvent carrying the polymer at the interface of the coagulation bath and the film are much higher, resulting in a dense toplayer as well. This ultimately hampers rapid outflow of the solvent, which in turn favours the formation of a porous structure underneath. Moreover, as a consequence of the formation of fingerlike pores, too large conical voids can be obtained in the submm range. These are so-called *macrovoids*, which can be almost as large as the film, shown in figure 2.3a. Denser means less permeable and the occurrence of macrovoids leads to loss in mechanical strength of the membrane.[2, 5, 9]

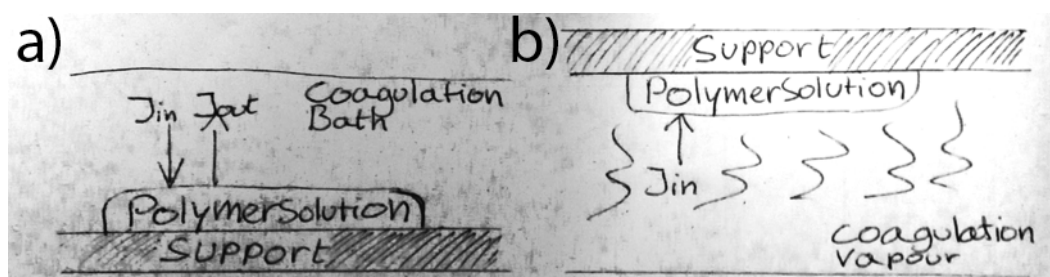


FIGURE 2.2: schematic representation of a) PIP or b) IPV. The polymer solution consists of a polymer:solvent. J_{in} is the non-solvent flux into the solution and J_{out} the solvent flux out the solution in the coagulation bath.

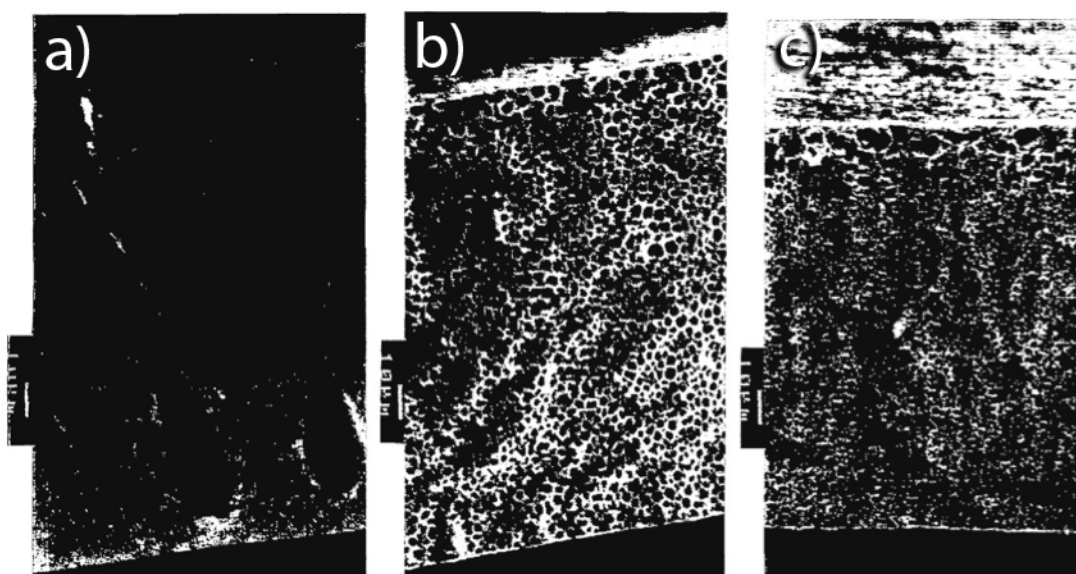


FIGURE 2.3: SEM cross-sections of a Polyetherimide (PEI) membrane obtained by: a) direct PIP. (take note of the macrovoids, almost as large as the film.) b) 5 min. IPV and PIP afterwards. c) PIP containing solvent:non-solvent = 90:10 wt%, E. Roesink (1989)[2]

Immersion precipitation from the vapour phase

To circumvent macrovoids and a dense toplayer it can be considered to apply Immersion Precipitation from the Vapour phase (IPV) first. The difference with PIP is that the polymer is coagulated by a steam bath. Thereby only indiffusion of the non-solvent takes place in the film and outdiffusion of the solvent is inhibited, shown in figure 2.2b. By applying IPV techniques a symmetric film of uniform pores can be obtained with the loss of macrovoids, shown in figure 2.3b.[2, 5, 9] In comparison to PIP, IPV results in a prolonged delayed demixing, but on the contrary faster to PI drying techniques. The latter causes the formation of dense non porous structures. Also other parameters during the PI technique can influence the formation of the membrane structure such as addition of solvent to the coagulation bath, shown in figure 2.3c, but lets first look to the actual processes going on during PI.

Processes during phase inversion

PI is a combination of *demixing* and *solidification*. First *demixing* occurs. Under influence of temperature or change in composition, the solvent demixes with the polymer, as the solvent is willing to mix with the non-solvent-e.g. the solvent of the solvent- but the polymer is not. Following polymer nuclei *coalescence* and form *aggregates* resulting in *solidification*. More precise the solidification process of a polymer can be separated in *gelation* and following *vitrification*. Gelation is the creation of a network of physically crosslinked polymer chains and the slow disappearance of the solvent still trapped in the network. with or without gelation present the polymer solidifies further by vitrification-e.g. glass formation. Depending on the nature of the polymer also *crystallization* can occur. The polymer rich concentration can than form a crystal network.[2, 5, 9]

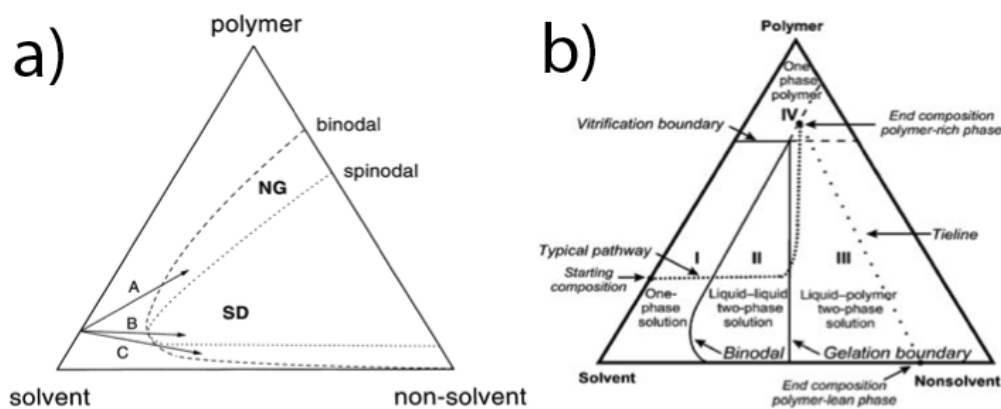


FIGURE 2.4: Two schematic ternary diagrams. In a) three different pathways are shown through the Nucleation and Growth (NG) area, indicated between the binodal and spinodal line and following the Spinodal Decomposition (SD) area. Pathway A only results in a porous structure, C. Barth et al. (2000)[3]. b) shows a typical pathway through the different phases of the system, L. Vogelaar et al. (2005).[4]

Ternary diagrams

Ternary phase diagrams as shown in figure 2.4 can be used to differentiate the demixing more precise for different systems that influences the forming of a porous structure. Demixing starts when a nucleus can form in the mixture, which occurs in the binodal phase (NG). The nuclei are not withstrained to grow further by cohesion until a thermodynamic equilibrium is reached at the tieline of the system. Spinodal Decomposition (SD) only occurs when the metastable region is passed and therefore does not occur during the formation of a membrane. In the binodal phase, the nucleation and growth can occur in a polymer rich (A) or -poor phase (C). With increasing polymer concentration the forming of a continuous polymer matrix is favoured. Formation of cylindrical pores occurs due to the presence of still polymer poor concentrations diluted in the mix. Thus a trade-off can be found. The binodal and spinodal regions in a ternary diagram depend on the interaction between the actual polymer, solvent and non-solvent. Low mutual infinity increases the magnitude of the demixing gap and vice versa.[3–5, 9]

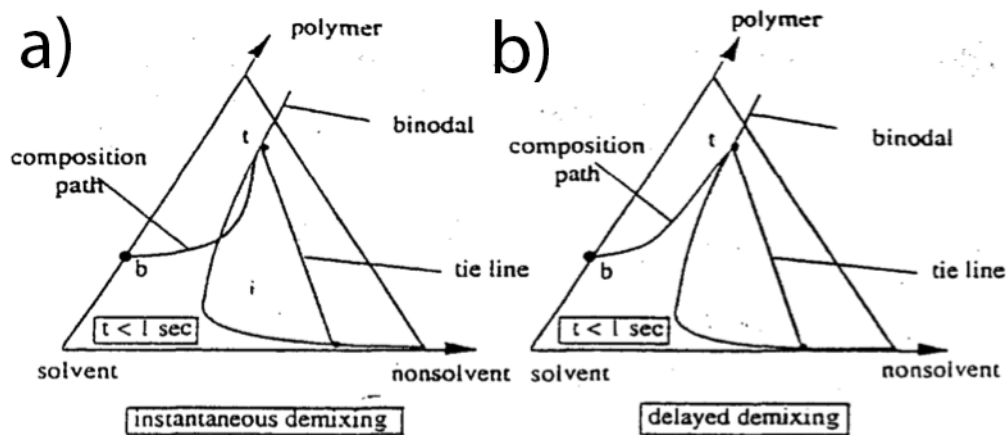


FIGURE 2.5: calculated initial composition paths in PIP for CA/dioxin/water system with varying initial volume fractions, J. Mulder (1996).[5]

Figure 2.5a-b show a composition path of a film/bath interface for instantaneous demixing and delayed demixing. t is the top and b is the bottom of the film. t is defined by the interaction parameters of the system. For instantaneous demixing the binodal is directly passed, indicating direct demixing. For delayed demixing the composition path stays longer in the homogeneous region and in a later time segment the binodal is also reached. Hence two different morphologies follow. By instantaneous demixing more of the film is within the binodal phase and therefore a more porous top layer is obtained. By delayed demixing this is not the case resulting in less dense toplayers.[5, 9]

Porosity enhancement techniques

Formation processes during PI and resulting porous structures of the membrane are dependent of several parameters of the production technique. The polymer:solvent:non-solvent system influences the interaction parameters and therefore the borders shown in the system can differ significantly. Main production technique parameters are described below.[2, 5, 9]

One of the main parameters needed to be considered is the choice of solvent:non-solvent. Higher mutual affinity favours instantaneous demixing by moving the binodal more close to the solvent in the ternary system, shown in figure 2.10. Table A.4 in *Appendix A* shows examples of combinations of solvent:non-solvent to attain microporous structures.

For micro- & ultra- compared to nano filtermembranes the porosity is mainly determined by choice of solvent:non-solvent. Nonetheless, the choice of polymer limits the actual solvents and non-solvents possible to use. As explained before, the mechanical, thermal and chemical characteristics of the polymer are important for other properties of the membrane such as rigidity and hydrophobicity, which influence porosity and fouling. Also polymer additives can be used to combine characteristics, such as hydrophilicity and rigidity.

With lower initial polymer concentrations, instantaneous demixing is favoured and also the polymer fraction in the membrane decreases resulting in higher porosity. Figure 2.6a shows an example of a calculated composition path for 20 % and 10 % initial polymer solution.

Next to increasing the temperature of the coagulation bath also addition of solvent can strongly influence the actual structure formed shown in figure 2.6b. Actually two opposing effects appear: Delayed onset of demixing tends to produce nonporous membranes with thick and dense top layers. On the contrary low polymer concentrations at the interface tend to produce more open top layers.[28]

The composition of the casting solution has also a considerable effect on membrane structure, shown in figure 2.6c. By adding non-solvent to the polymer solution the initial composition shifts closer to the binary line. Hereby delayed demixing systems can be transformed to instantaneous demixing systems.

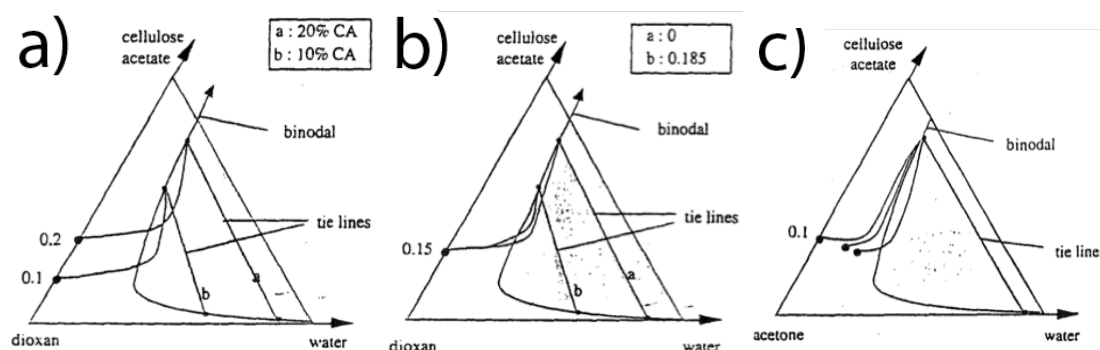


FIGURE 2.6: Schematic ternary diagrams with calculated composition paths for: a) CA/dioxin/water system with varying initial volume fractions, b) for the system CA/-dioxin/water with different fractions of dioxin in the CB & c) for the system CA/acetone/water with varying non-solvent content in initial solution, J. Mulder (1996)[5]

Summary: Porosity enhancement methods

SEM photographs in figures 2.1 & 2.3 show that for different PI methods and preparation methods, the resulting membrane can differ substantially in structure-related properties. Parameters affecting permeation-related properties are directly dependent of the polymer or additives used. By applying IPV instead of PIP a dense toplayer can be circumvented. Hence concerning basic membrane science literature the following enhancement methods can be applied to promote porous membrane structures:[2, 5, 9]

- Lower initial polymer concentrations.
- Higher mutual affinities between solvent:non-solvent.
- Increase temperature CB.[28]
- Addition of non-solvent to the polymer solution (controversy exist). [28]
- Polymer additives to combine polymer characteristics. [29]
- Post-treatment: Heating, grafting, coating or grinding (not discussed).
- Use support as mold, to attain micro surface structures (not discussed).[4, 33]

2.2 Selecting the right binder for PI produced FeS anodes: PVDF vs. PES

Above it is mentioned that solely pore properties affect permeation of microfiltration membranes. In contrast, both polymer- and pore properties influence ionic conductivity of a microporous electrode in aquatic solution.

Hydrophobicity

An important parameter of polymers to begin with is hydrophobicity. It can decrease permeability of a membrane and tends to favour attachment of particles-e.g. fouling of membranes.[34] Considering the electrochemical performance, an hydrophobic binder could than restrain ionic conductivity in an aqueous battery.[8] On the contrary, it also might mean higher overpotential of the water/hydrogen couple, inhibiting the HER. A very hydrophilic polymer is Cellulose Acetate and very hydrophobic polymers are Polypropylene (PP) Polyethylene (PE) and Polytetrafluorethylene (PTFE). Less hydrophobic PVDF, PES, Polysulfone (PS) and Polyacrylonitrile (PAN) exists that can be tweaked to some extent in hydrophilicity by using additives or a post-treatment. T. van Dijk (2012) also mentions Sulphides are expected to dissolve in the electrolyte.[8] Therefore it is not necessary to apply pore forming additives.

Mechanical-, chemical- & thermal strength

Other parameters that are intertwined with hydrophobicity are mechanical- thermal- and chemical- resistance. PIP can be applied when a polymer is miscible-e.g. CA, PVDF, PES, PS and PAN. In general being hydrophilic or having a solvent goes hand in hand with a decrease in mechanical, thermal and mechanical strength. CA is limited in pH resistance and susceptible for hydrolysis. On the other hand, PP, PE, PTFE are excellent in strength but are limited in blend capability. These can only be used for dry spinning techniques, which create low porous slit like structures and cannot be applied for production techniques to create circular porous structures as PIP and IPV. PE can be made hydrophilic by post treatment, but surprisingly they are not common used microfiltration products. On the other hand PP is used for microfiltration membranes but cannot be made hydrophilic.[34]

Electrochemical performance of Fe(S) anodes depending on choice of polymer

PVDF and PS are most common used polymers for PIP filtermembranes, both due to their extraordinary mechanical-, chemical- and thermal resistance.[34] Although both polymers are electrical insulators, PVDF and PS are known in the electrochemical industry as binders for in electrodes. [5, 35] Traditional production techniques can be used to create electrodes with PVDF as binder by sintering and pressing. To be even more specific, E-stone Batteries have researched pressed electrodes with PVDF and sintered electrodes with PTFE as binder but showed worse results compared to pure pressed pills.[8] Kitamura et al. (2012) compared the effect of 10 wt% binder on the cycling performance of ferric oxide (Fe_2O_3) dried anodes. Anodes having PTFE and PE showed best performance, having capacities of 500 mAh/g for 100 cycles with 80 % energy efficiency, by cycling on both plateau's. Anodes having PVDF and P-TFE-VDF as binder

performed worst.[24] A probable explanation for the bad performance of fluorinated polymers is given in section 2.2.1.

Applicable phase inversion polymers for a FeS anode

In contrast to PE and PTFE, PVDF and PS both consider good miscibility in some solvents. Therefore PS and PVDF can also be used for PI techniques. Following literature this thesis introduces the possibility of PES, family of PS, as polymer binder for FeS anodes. In table 2.1 an overview is given of the characteristics of Kynar Flex[®] PVDF and Ultrason 6020P[®] PES in mechanical-, chemical- and thermal resistance, electrical conductivity, hydrophilicity, solvability, flexibility, toxicity and degradability.

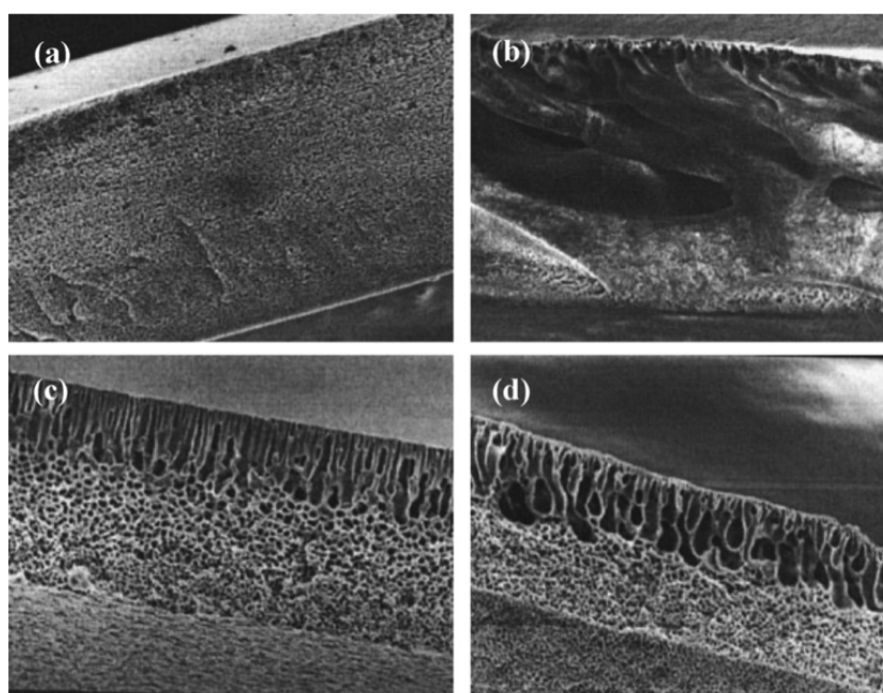


FIGURE 2.7: SEM cross sections of membranes by PIP with the system PVDF/solvent/water having solvents: a) TEP, b) NMP, c) DMF and d) DMAc. Higher solubility of PVDF in the solvent increases porous structure of the resulting membrane, K. Wang (1989).[6]

2.2.1 PVDF

Properties

PVDF is a semi-crystalline thermoplastic polymer, consisting of a $-\text{CH}_2\text{-CF}_2-$ repeating structure. Due to the c-c structure it has high flexibility. Depending on the spatial arrangement of the CH_2 and CF_2 groups along the polymer it can crystallize between 35-70 %. By PIP usually a symmetric membrane can be obtained with uniform spherical PVDF crystallites. Due to the fluorinated side groups and crystalline behavior, PVDF

exhibits excellent mechanical strength, thermal stability and chemical resistance compared to other commercialized polymeric materials, having a T_m of 140-170 °C and T_g of -41--38 °C. However the chemical resistance does not apply for strong base solutions, esters or ketones. In presence of one of these, neighbouring -H and -F side groups can dehydrofluorinate, whereby HF and a C=C bond forms in the main chain, resulting in further loss of inertness for stress and temperature. When adding 6M KOH (aq) to the surface of the membrane a direct colourization occurs, which is sign of the initiated C=C bonding. An experiment of a pure PVDF laminate in 6M KOH indicates this new state is less flexible but still rather stable for four months already. A critical note is the forming of KF out of HF in the solution, which is known to be very corrosive. PVDF is relatively more hydrophobic compared to PS and PES. Commercially available PVDF exists in the form of homopolymer Kynar[®] and copolymer Kynar Flex[®]. In general, using a copolymer improves miscibility by solvents compared to using a homopolymer but will also result in a lower mechanical strength. Due to its crystallinity its behavior during PIP is more complicated than for an amorphous polymer such as PES. PVDF solvents with highest mutual affinity are DiMethyl SulfOxide (DMSO), DiMethylFormamide (DMF), HexaMethylPhosphorAmide (HMPA), N-Methyl-2-Pyrrolidone (NMP) and TriEthyl Phosphate (TEP). Resulting structures using different solvents are shown in figure 2.7. The effect of a different non-solvent is shown in figure 2.8. Water has a higher surface tension than ethanol and therefore induces rapid demixing resulting in a fingerlike porous structure. By using ethanol a symmetric non-porous structure is obtained. Figure 2.10a shows a ternary diagram for the system PVDF/NMP/non-solvent at 25 °C. Water has the highest mutual affinity. Known pore former additives for PVDF are low molecular weight inorganic salts-e.g. LiCl, LiClO₄. Additives as polymers-e.g. PolyVinylPyrrolidone (PVP) M_w 10.000, PolyEthyleneGlycol (PEG), PolyMethyl MethAcrylate (PMMA)- and other types of additives-e.g. Glycerol, water, 1,2-ethanediol- increase hydrophilicity and thereby also porosity. Nonetheless additives are not common for PVDF because they favour macrovoid formation and therefore a weakening of the mechanical strength. [6, 34]

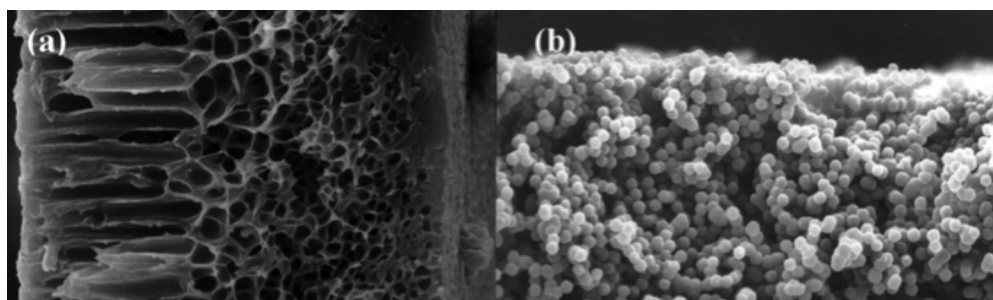


FIGURE 2.8: SEM crosssections of membranes by PIP with the system PVDF/DMF/non-solvent having non-solvent: a) water and b) ethanol. Higher affinity between solvent/non-solvent increases porous structure, K. Wang (1989)[6]

2.2.2 PES

Properties

PES is a thermoplastic amorphous polymer, consisting of an oxide-diphenylene-sulfone repeating structure. The C-S bond in the main chain causes the polymer to be flexible. The -SO₂ group has electronic attraction of resonating electrons between adjacent aromatics groups and is therefore quite stable. The oxygen molecules each have two pairs of unshared electrons to donate to strong hydrogen bonding, causing good solubility. The repeating phenylene rings contribute to its high rigidity, strength, creep resistance, dimensional stability and heat reflection temperature. PES therefore has very high thermal and oxidative stability with a T_g of 225 °C, producing long-term, high temperature stability during use. PES has excellent chemical resistance to chlorines, aliphatic hydrocarbons, fully halogenated hydrocarbons, alcohols and acids, excluding aromatic hydrocarbons ketones, ethers and esters, which is pretty similar to PVDF. The pH tolerance is said to be from 1-13.[36] Experiment of a pure PES laminate in 6M KOH (aq) indicates stability for four months already. Barth et al. (2000) shows that for the system polymer/DMF/water, the resulting PES membrane has more fingerlike pores than PS as a result of the more polar nature and higher affinity to water. Therefore PES ought to be more suitable for liquid separation.[3] The effect of lower initial concentrations and addition of acetone for the resulting membrane are shown in Figure 2.9. Figure 2.10b shows the ternary diagram for the system PES:solvent:water.[7] It can be seen that PES has a most high mutual affinity for DMSO and DMF. PES is still highly hydrophobic but less than PVDF. However the good solubility of PES causes the polymer to be ideal for blending with additives-e.g. PVP, PEG and Pluronic (Plu)- to attain hydrophilic polymers with the advantages of PES; having good mechanical, chemical and thermal resistance.[34] H. Susanto (2009) indicates that PES-Plu- show higher permeability and PES-PVP blend highest hydrophilic behavior than PES-PEG but stresses that the stability of the additive is a critical problem. Concluding PES-Plu blend has the highest stability.[37] By adding solvent to the initial solution the morphology of a membrane can be influenced as well. Xu (2004) shows that for the system PES/NMP/water the resulting membrane morphology changed slowly from long and wide to thin fingerlike structure and following sponge-like structures by increasing ethanol concentration in the initial solution.[38]

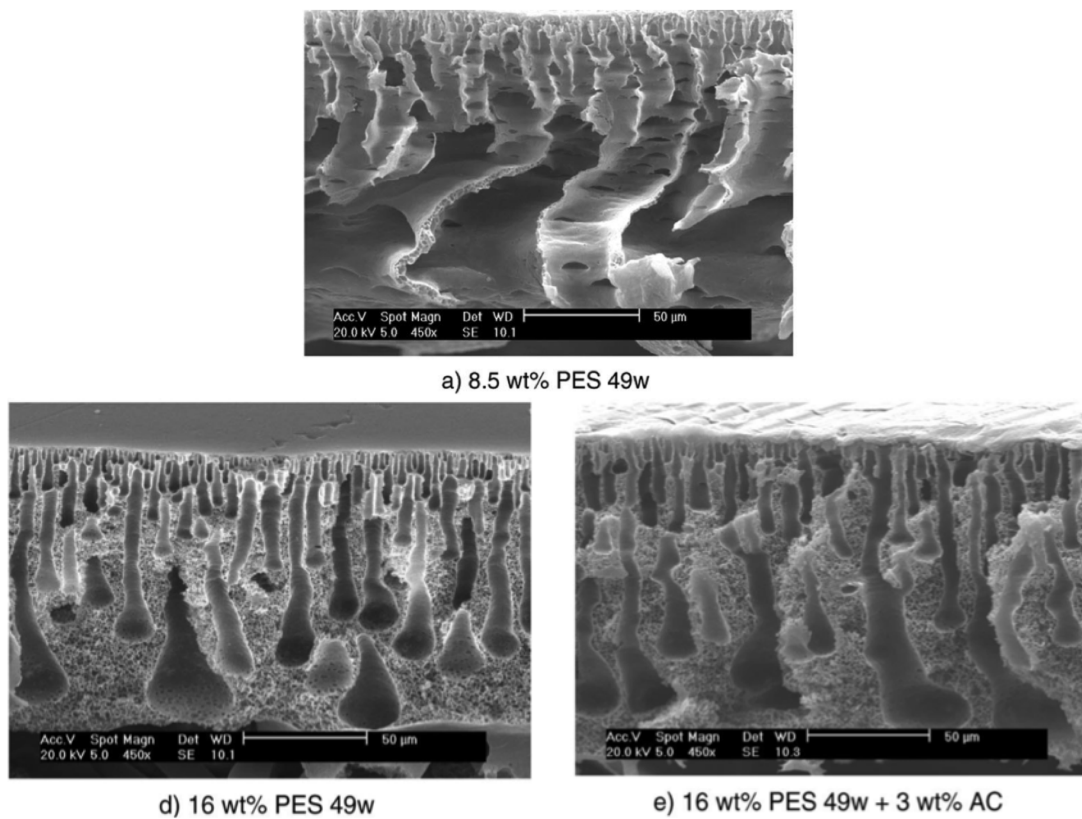


FIGURE 2.9: SEM cross sections of membranes prepared by the system PES 49w/DMF/H₂O, C. Barth (2000).[3]

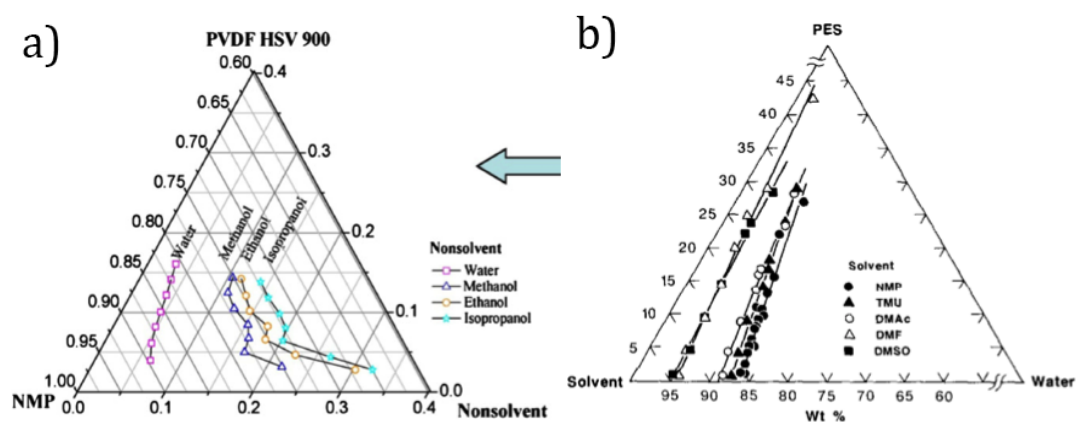
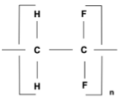
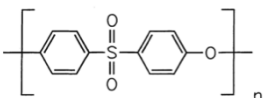


FIGURE 2.10: Ternary diagram showing the binodal for the system a) PVDF/NMP/non-solvent for different non-solvents, K. Wang (1999) and b) PES/solvent/water for different solvents, W. Lau (1991).[6, 7]

TABLE 2.3: Properties of PVDF and PES

<i>Polymer</i>	Kynar Flex 2801[39]	Ultrason E6020P[40]
<i>Supplier</i>	Arkema Inc.	BASF
<i>Type of polymer</i>	Copolymer	
Physical properties		
Density (g/ml)	1,76-1,79	1,3
Water absorption (%)	0,03-0,05	0,0
Mechanical Properties		
Tensile stress at yield (MPa)	20-34	85
Tensile stress at break (MPa)	17-34	
Elongation at yield (%)	10-20	6,9
Elongation at break (%)	200-400	
Elongation at break (%)	551-896	2.650
Thermal Stability		
T _m (°C)	140-145	225
T _g (°C)	-42-39	
Thermal stability 1wt% loss in air (°C)	707	
Electical Properties		
Dielectric Strength (kV/mm)	1,3-1,6	
Dissipation factor (100Hz)	001-0,22	
Volume resistivity (Ωcm)	2 10 ¹⁴	
Total Solubility parameter (MPa		
DMSO	26,7	
DMF	24,8	
HMPA	23,2	
NMP	22,9	
PVDF vs PES [34]		
Polymer costs	-	+-
UF rating	+-	+
Permeability	+-	+
Caustic resistance	+-	+
Chlorine resistance	+	+-
Alkaline resistance	-	+
Feed range	+	+-
Fibre breaks	-	+-
Membrane life	+	+++
Structure		
		

Chapter 3

Porosity enhancement methods for PVDF

The first experiment is to test and quantify the achievement of porosity of pure polymer membranes by different porosity enhancement methods discussed in chapter 2. The enhancement methods investigated for the system PVDF/NMP/water are: PIP vs IPV, increase in temperature of CB and addition of solvent in CB. Attainment of porosity must not delimit the strength of the polymer obtained. Therefore the strain strength of the membrane is shortly investigated as well. NMP is considered as toxic. DMSO is less toxic showing an even higher solubility parameter for PVDF. Hence, considering the sustainable aspirations of E-Stone Batteries, also the system PVDF/DMSO/Acetone/water is investigated, with DMSO/Acetone = 90:10 wt%. The increase in porosity is determined by looking to the shrinking during membrane formation and following, change in thickness and density.

3.1 Experimental section

Kynar Flex LBG[®] is kindly supplied by Arkema, specifications are given in chapter 2. NMP, DMSO and Acetone are obtained via Sigma-Aldrich.

Films of 0,5 mm are casted on a clean glass support. When PIP is applied the film with its support is directly immersed in its CB. If not mentioned otherwise the CB is tap water. When IPV is applied, demineralized water is boiled at 100 °C and the resulting steam is directly applied on the thin film by placing it above the boiling water. When the film looks miscible the film with its support is immersed in the CB, which generally takes 30 seconds.

To determine the density a 13 mm circle is punched out of a membrane and the resulting pill its thickness (t) and weight (g) are measured. The density is then obtained as follows

$$\rho(g/cm^3) = \frac{g}{\pi r^2 t} \quad (3.1)$$

where r is the radius of the pill. An indication of the pore space $PV_{\Delta t}$ and $PV_{\Delta \rho}$ in the membrane is calculated by respectively

$$PV_{\Delta t}(v\%) = \frac{(t - t_{initial}) \frac{g_{polymer}}{g_{polymer} + g_{solvent}}}{t} \quad (3.2)$$

$$PV_{\Delta \rho}(wt\%) = \frac{1 - \rho}{1 - \rho_{polymer}} \quad (3.3)$$

assuming $wt\% = v\%$, $t \ll$ width and length of the casted slurry and there is no solvent or non-solvent left in the membrane. In fact, there will be non-solvent and solvent left in the membrane also influencing the density. Therefore $PS_{\Delta t}$ is seen as a better indication of the pore space.

An order of the strain strength is investigated by attaching two cramps on both sides of the membrane in casting direction and applying increasing strain stress on it by hand. Following the strain stress is obtained by using analog newtonmeters. Determination of strain stress for each sample is repeated two times. The breaking stress (BS) is calculated using

$$BS(N/m^2) = \frac{F_{max}}{wt} \quad (3.4)$$

where F_{max} the stress needed to break the membrane and w the width of the membrane, neglecting the influence of stretch speed.

3.2 Results & discussion

Figures 3.1a-d show the thickness and density of PIP and IPV membranes for different temperatures of CB's and different PVDF:NMP concentrations. The black plots in figures 3.1a & b show calculated thickness of pure PVDF membranes out of the initial casting thickness of 0,5 mm, whereas the black plots in figures 3.1c & d show calculated densities for the plotted PVDF:NMP concentration. Depicted in table 3.1 are indications of pore space in v% & wt % for membranes by different enhancement methods. Regarding thickness, PIP membranes maintain around the same order, in comparison to the initial casting thickness, which is between 0,25-0,41 mm, indicating a pore space of 83 v% for 12 wt% PVDF. Using IPV the resulting laminate is a factor 5 thinner,

between 0,10-0,20 mm and an estimation of 50v% pore space for 12 wt% PVDF. Also, for PIP, an increase in thickness with decreasing initial concentration, while for IPV, a smaller decrease in thickness with decreasing initial concentration can be observed. The calculated densities seem to follow the experimental results, while for IPV the density of the results are higher than the densities calculated. This suggests a decrease in pore space when IPV is used instead of PIP. Moreover, the big difference in pore volume of 30 v% could be a sign of macrovoid formation. An overall negligible small influence of temperature change can be seen for both techniques.

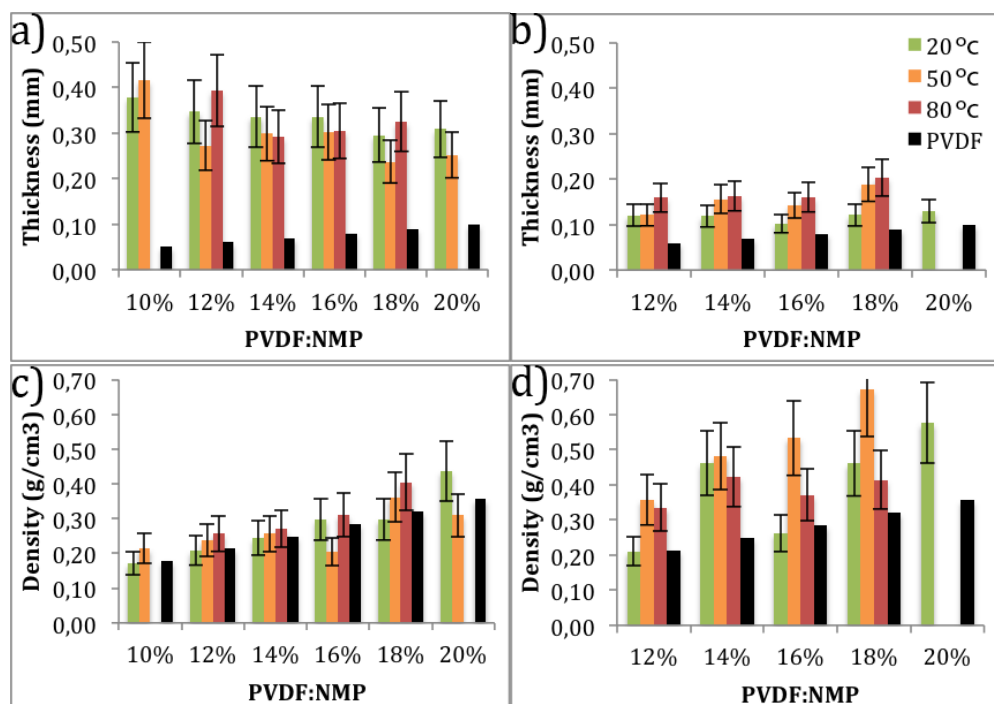


FIGURE 3.1: Thickness and density for different initial concentrations PVDF:NMP (wt%) for PIP- & IPV membranes, respectively shown above and below. The different coloured plots indicate the temperature of CB used. The black PVDF plots show the calculated thickness and density of membranes following the PVDF:NMP concentration of the solution.

Figure 3.2a & b show the thickness and density of PIP and IPV membranes for different initial concentrations PVDF:NMP (wt%) when adding 10 wt% solvent to the CB. Figure 3.2c & d show the same parameters but than for different solvents used: DMSO vs. NMP. For PIP membranes, by adding solvent to the CB no significant difference can be found in change in thickness and density. For IPV membranes the thickness increases by adding solvent to the CB resulting in an increase in pore space of 67 v% for 12 wt% PVDF. Regarding using different solvents not a significant difference can be obtained in density nor thickness but more data is needed to be more concise.

What can be expected of the mechanical strength of a membrane is that lower initial concentrations cause higher porous volume and following the membrane to break at lower

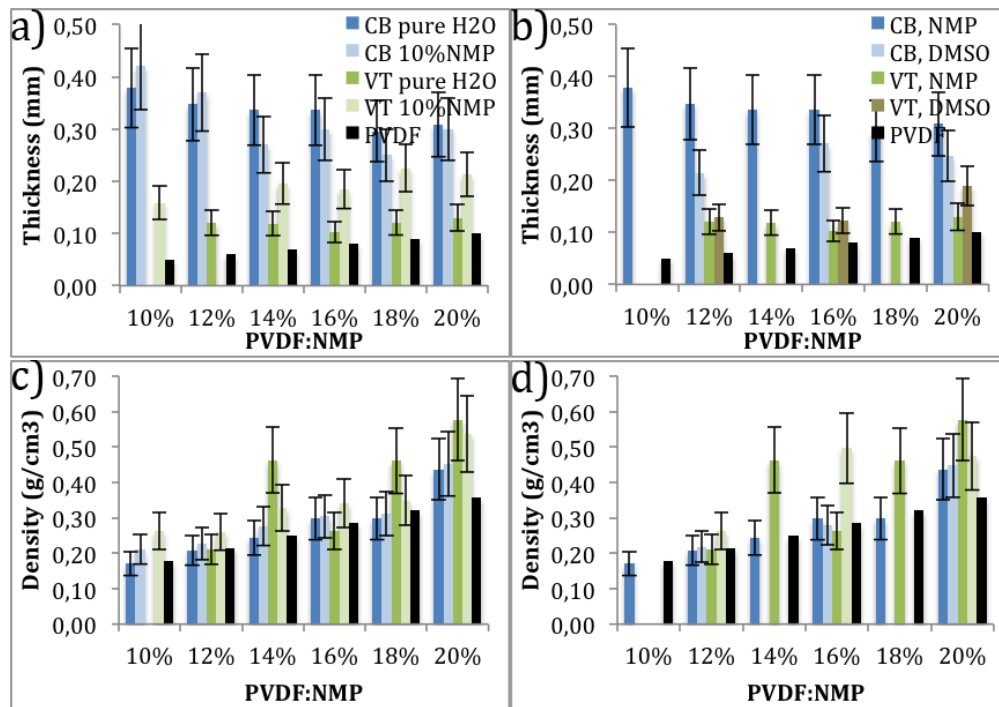


FIGURE 3.2: Thickness and density for different initial concentrations PVDF:NMP(wt%) when adding 10 wt% solvent to the CB and the use of DMSO is compared to NMP. The black PVDF plot shows the thickness and density following the PVDF:NMP concentration of the solution. CB & VT means respectively PIP and IPV.

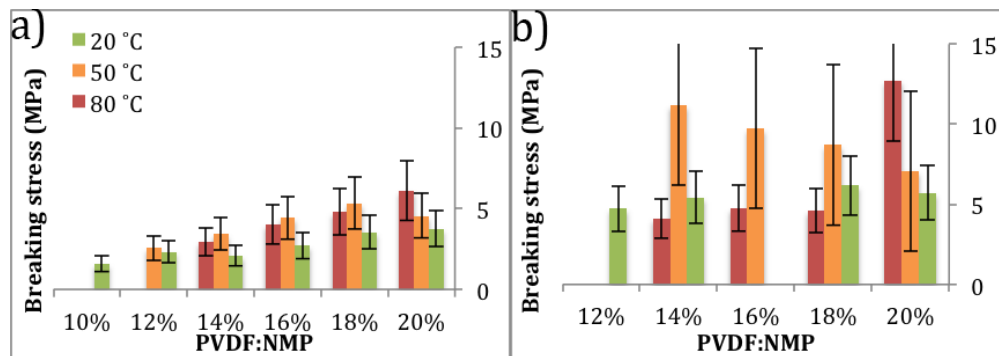


FIGURE 3.3: Breaking stress for PIP and IPV at different initial concentrations PVDF:NMP (wt%).

stress. Figure 3.3a-b show breaking stresses for PIP & IPV membranes at different initial concentrations. Indeed, for PIP an increase can be observed in stress needed to break the membrane from 1-5 MPa. The breaking stress for IPV is an order higher from 5-10 MPa. Apart from and maybe also due to some outflows, for IPV membranes no correlation between initial concentration and breaking stress can be observed.

Appendix B shows the effect of an oven post-treatment. It can be seen that heating of the membrane initiates further vitrification, whereby the polymer shrinks and the density increases, which indicates loss of pore volume.

3.3 Conclusion

By applying PIP using low initial PVDF concentrations of 12 wt%, very high porous structures can be obtained of around 83 v% in comparison to 70 v% for high initial PVDF concentrations of 18 wt%. However the possible formation of a dense top layer can negatively affect the permeability of the membrane. Before PIP an IPV treatment can be applied to have a more porous top layer but causes the porosity to decrease to 50 v% for initial PVDF concentrations of 12 wt%. On the other hand, an IPV treatment positively affect mechanical strength probably due to the loss of macrovoids. Enhancement method by using higher temperatures for CB or add solvent to the CB show for this experiment insignificant increase in porosity. Noticing is that only for IPV an increase in porosity of 17 v% can be observed by adding solvent to the CB. Using DMSO instead of NMP show insignificant differences in porosity as well. A post-treatment is said to break open the pores of PIP membranes. Caution needs to be taken for too much vitrification, resulting into loss of porosity.

TABLE 3.1: An estimation of pore volume using different enhancement techniques looking to Δt & Δq

<i>System</i>	PVDF (wt%)	NMP:H2O(20 °C)		NMP:H2O(50 °C)		NMP:H2O(80 °C)		NMP:H2O:NMP(10 wt%)(20 °C)		DMSO:H2O	
<i>Technique</i>		PIP	IPV	PIP	IPV	PIP	IPV	PIP	IPV	PIP	IPV
$PV_{\Delta t}$	12	83 %	50 %	78 %	51 %	85 %	62 %	84 %	67 %	72 %	53 %
$PV_{\Delta q}$		88 %	88 %	87 %	80 %	86 %	81 %	87 %	85 %	88 %	85 %
$PV_{\Delta t}$	18	70 %	26 %	62 %	52 %	72 %	56 %	64 %	60 %	65 %	42 %
$PV_{\Delta q}$		83 %	74 %	80 %	62 %	77 %	77 %	83 %	80 %	80 %	73 %

Chapter 4

Porous membranes as FeS electrode support

For optimal ionic conductivity it is favorable to have thin membranes consisting of porous morphologies to enhance the accessibility of active material within electrodes. As depicted on the cover of this report and mentioned in Chapter 1, in theory, fingerlike macroporous structures surrounded with micro- and mesopores are ideal for optimal electrochemical behavior. In chapter 3 PIP and IPV porosity enhancement techniques have been examined. In this Chapter, the porous structures of polymer membranes with the addition of submicron active material particles to the initial polymer solution will be investigated. Most importantly how and if PVDF and PES carry FeS. Different amounts of FeS are added to the polymer solution and the porous structures that are created by IPV or PIP. The resulting membranes are examined using SEM imagery of cross-sections and surfaces and density pycnometry analysis. SEM cross-sections provide information of the solidification and distribution of FeS within the laminate and the sizes structures and -morphologies of the pores while surface SEM imagery elucidate the achievement of an open porous top layer. Pycnometry analysis can then quantify the achievement of continuous open pores.

4.1 Experimental section

PVDF Kynar Flex LBG[®] and PES Ultrason E6020P[®] are happily supplied by Arkema and BASF, specifications are given in Chapter 2. C-ENERGY[®] SUPER P and TIMREX[®] SFG15 Graphite are kindly supplied by IMERYYS. FeS, NMP, DMSO, Acetone and Nickel are obtained via Sigma-Aldrich.

For production specifications of PIP and IPV films, see the experimental section of Chapter 3.

Throughout all experiments it is intended to use the same FeS particle size and distribution. This is done by ballmilling in zirconium oxide 150 ml cups at 250 RPM for eight times fifteen minutes using a weight content:ball ratio of 1 %:50 %. The ballmilled active material FeS are expected to be in submicron range. SEM imagery of ballmilled particles, shown in Appendix C confirm particles of 100 nm are achieved but also a wide distribution of sizes can be found with also bigger clumps of 50 μm . Due to van der Waals forces ball milled FeS particles smaller than $< \mu\text{m}$ have a tendency to form clusters, similar to the clumps observed on the SEM pictures.[41] Hence FeS particles are expected to be much smaller ball milled than the clumps observed.

The ballmilled FeS particles are subsequently mixed with the solved polymer using a homogenizer for 10 minutes with a 11 mm head in a 5 ml cup. The initial solution is mixed 10 % PVDF in solvent and 8 % PES in solvent, the rate of fill is 5 % polymer:active material:conductive material. If not mentioned otherwise, the above mentioned parameters are considered as fixed.

SEM pictures of films are taken at Twente University using a gold substrate and at TU Delft using a carbontape substrate. Films investigated are in the order of 0,2-0,4 mm. SEM specifications are given below in the respective figure.

Density analysis have been performed for all cells tested at E-Stone Batteries using equation 3.3. Moreover at the University of Amsterdam a volume analysis have been performed using a gas pycnometer. The gas used is helium and the determination of each sample have been performed eight times using

$$\rho(g/cm^3) = \frac{g}{V_c + \frac{V_r}{1 - \frac{P_1}{P_2}}} \quad (4.1)$$

with V_S the sample volume, V_C the volume of the empty sample chamber, V_r the reference volume, P_1 the initial pressure and P_2 the pressure after expansion

4.2 Results & discussion

4.2.1 SEM cross-sections of PIP membranes compared

Depicted in figure 4.1 are cross-sections of PIP membranes consisting of a) 25 % FeS:PVDF, b-d) show FeS/PES with increasing FeS content ranging from 25 %, 50 % to 95 %. All percentages given are weight percentages. For 25 % and 50 % FeS ratios the typical

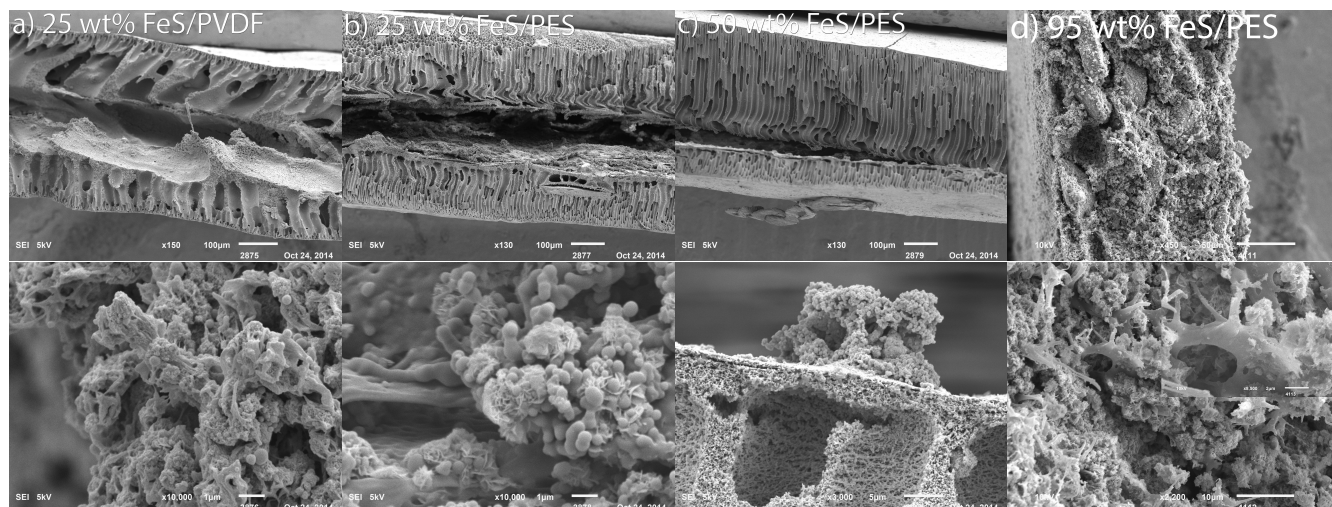


FIGURE 4.1: Above SEM cross-sections and below an enlargements of PIP membranes are shown by the system a) FeS/PVDF/NMP/H₂O, 25 % FeS/PES. b) FeS/PES/NMP/H₂O, 25 % FeS/PES. c) FeS/PES/NMP/H₂O, 50 % FeS/PES. For all preceding, the initial concentration is 20 % PES/solvent. d) FeS/Super P/PES/90 % DMSO/10 % acetone/H₂O 80 % FeS/15 % Super P/PES, Initial concentration is 10 % PES/solvent.

finger like porous structures can be observed. The PVDF membrane shows bigger finger like pores than PES. This could be due to the tendency of PVDF to favour macrovoid formation explained in Chapter 2. Small angular formed particles in the submicron range can be observed within the finger like pores. Spectrum analysis indicates these are FeS containing particles. A bigger distribution of particles can be observed in 50 % PES. During the coagulation, the film broke up in two. The resulting junction in the middle of the laminates shows a more rough surface, which could be a sign of differentiated FeS on the junction of the polymer. Looking to the enlargements, spherical particles can be found with strokes surrounding the particles, especially this can be seen on figure 4.1b. Figure 4.1c shows ceased aggregate forming of globular particles on top of the film. Spectrum analysis indicates that the strokes are FeS particles and the more spherical black formations are the binder.

Anodes acquired by direct pressing of FeS powder have the tendency to break due to their fragility. Therefore binder is usually added up to 10 %. The implementation of a CB enables the creation of more rigid electrodes. Figure 4.1d shows a membrane consisting of solely 5 % binder while still being rigid. It is suggested even lower amounts of binder can be added while still remaining solid and rigid. Typical finger like porous structures cannot be found using 5 % binder. Instead a more homogeneous morphology is obtained. Nonetheless still a porous support is successively obtained with ultra- to macroporesizes of 0.1-15 μm , containing captured and dispersed FeS particles. In contrast with figures 4.1a-c big chunks can be found as well. These chunks are comparable to the aggregate forming in appendix C. A possible explanation could be that a less

homogeneous mixture of the casted slurry is produced by using a homogenizer instead of a planetary mixer, which is used for the 25 % and 50 % FeS polymers. In figure 4.1a and c the typical dense top layer can be found on one side of the film. The bottom layer also shows a dense layer but is more thin than the top layer. From figure 4.1d it does not become clear if a dense top layer exists. SEM analysis of the surface could give more clarification. Unfortunately, no SEM imaging exists in this thesis of laminates having FeS/polymer ratios between 50 % and 95 %. To obtain proficiency in the maximum of polymer ratio needed to obtain still finger like porous structures, it is interesting to make more SEM imaging in this range as well.

4.2.2 SEM cross-sections of IPV membranes compared

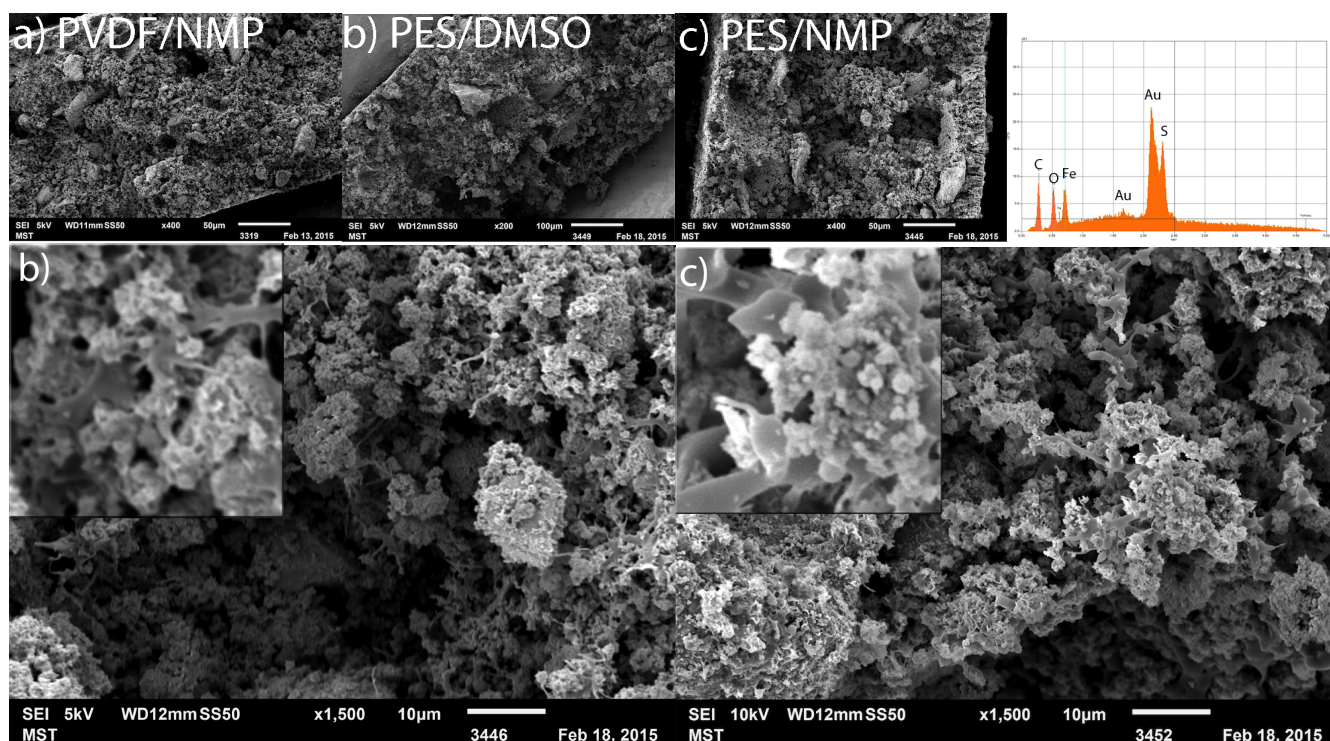


FIGURE 4.2: SEM cross sections of IPV films produced by the system a) FeS/PVDF/DMSO/H₂O resulting in the laminate 95 % FeS/PES, b) FeS/PES/DMSO/H₂O resulting in 95 % FeS/PES and c) FeS/PES/NMP/H₂O resulting in 95 % FeS/PES. The figures below show enlargements of the above.

Depicted in figure 4.2 are cross-sections of IPV films produced by the system a) 95 % FeS/PVDF/NMP b) 95 % FeS/PES/DMSO and c) 95 % FeS/PES/NMP. Below enlargements are given and for the enlargement of c) an elementary analysis is included. Also by applying IPV an homogeneous porous structure is obtained with microporesizes of 0.1-10 μm . Comparing the amount of black spots in IPV to PIP laminates it seems the PIP laminate from figure 4.1d has more pore volume than both PVDF and PES membranes. Moreover, for IPV with high ratio of FeS, the spot analysis indicates that

FeS indeed occurs within the membrane. Similar to high ratio FeS PIP membranes, big chunks of FeS can be found as well, suggesting better homogenizing of the slurry is needed to obtain a more homogenous structure. From the enlargements a round shaped entangled branched structure can be observed with within more white globular particles ranging around $0,5 \mu\text{m}$. Spectrum analysis indicates these particles are FeS carried by PES polymer support. If pores are achieved in the ultra-range can not be concluded from the SEM enlargements. Therefore a porosity experiment using BET-analysis is advised to assess this. By doing so it is also interesting to acknowledge information of the occurrence of macro- micro- and ultrapore formation between PVDF and PES membranes.

4.2.3 SEM surface imagery of membranes & pressed pills compared

Figure 4.3a-b show SEM imagery for the top surface of a PIP membrane consisting of respectively a) 25 % FeS/PVDF and b) 25 % FeS/PES. As expected from PIP a dense nonporous top- as well as bottom layer is obtained. The PVDF laminate shows a wrinkle effect of the surface due to the shrinkage of the film, which is in alignment with macrovoid formation observed from the SEM cross-section ??a. PIP membranes containing 50 wt% FeS show some submicron particles can be found on the bottom layer, which are probably FeS. Also for PES a nonporous surface can be observed. However, the middle-junction surface shows an open structure with tubular macropores with a diameter of around $15 \mu\text{m}$ surrounded with small pores with a diameter of $0,5 \mu\text{m}$. This is similar to the optimal porous structure for electrodes, proposed in Chapter 1. Within these smaller pores it is interesting if smaller pores exists within the ultra-range as well

IPV and PIP membranes containing 95 % FeS and 5 % PES both show white rough particles encapsulated by long strokes of black circular formations including open porous structures. Spectrum analysis indicates the former to be FeS particles and the latter polymer. A x2200 and x8500 enlargement is done to indicate the occurrence of pores respectively in the micro- and ultra-range. IPV has surface pores from 1-6 and $0,5-1 \mu\text{m}$, while PIP seems to have smaller pores 1-1,5 and $0,3-1 \mu\text{m}$. On the contrary for IPV the FeS particles seem to be more coagulated than using PIP. For comparison figure 4.2e shows the surface of a pressed pill containing FeS/Super P/PVDF in the ratio 82:10:8 %. It must me emphasized no pore former techniques have been used. Some slitlike pores can be found in the range of $0,5\mu\text{m}$, which is smaller than is obtained using PIP or IPV techniques. Surface SEM imagery of PIP and IPV membranes can give more insight in the achievement of an open porous top layer.

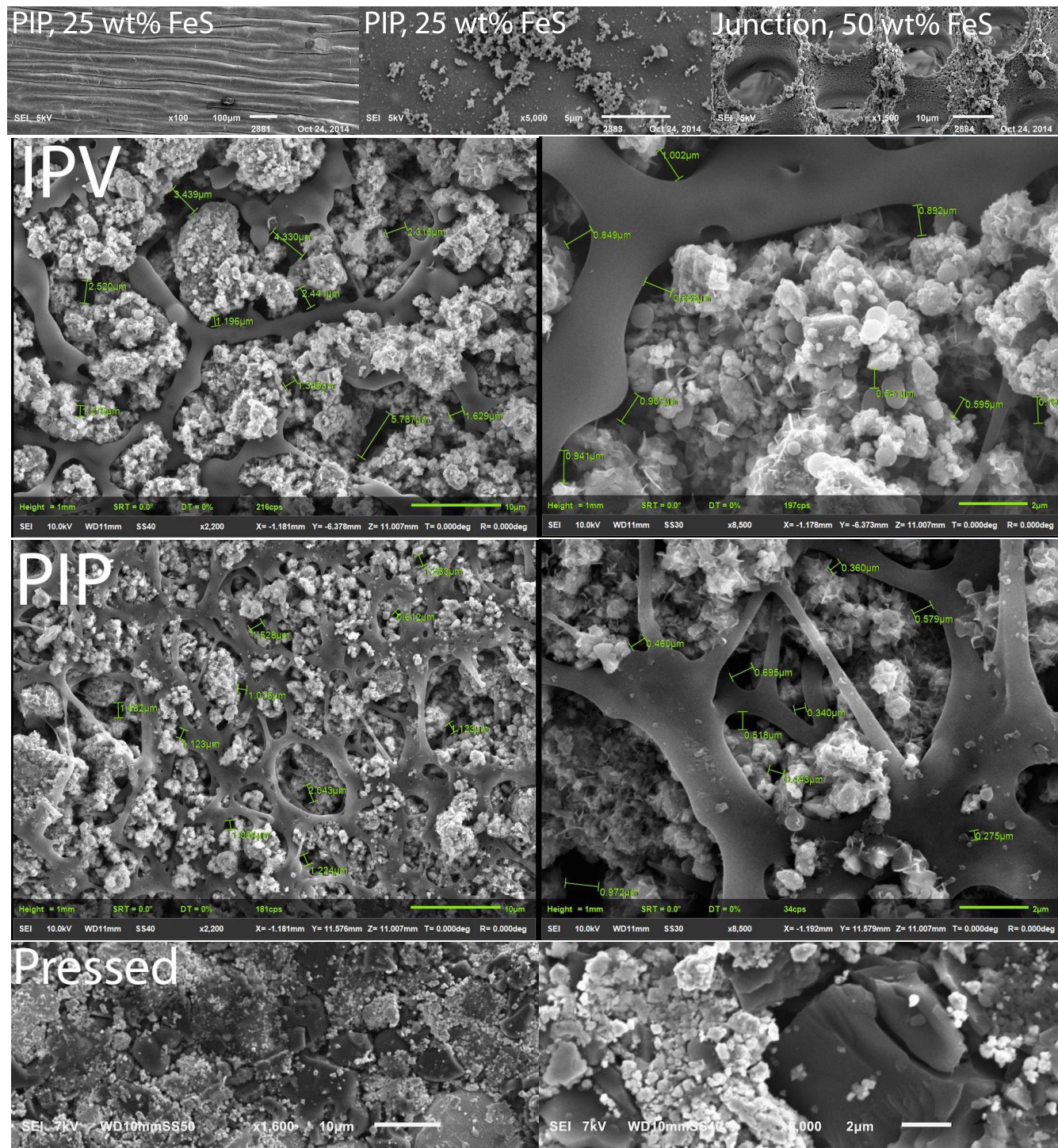


FIGURE 4.3: SEM toplayer surface imagery of membranes. PIP, 25 wt% FeS/PVD-F/NMP/H₂O. PIP, 50 wt% FeS/PES/NMP/H₂O, shows the bottom layer. Junction, 50 wt% FeS/PES/NMP/H₂O. IPV and PIP are made by the same system 95 wt% FeS/PES. The pressed pill contains FeS/Super P/PVDF in the ratio 82:10:8 wt% .

4.2.4 Pore space analysis of PIP & IPV membranes & pressed pills compared

To quantify the achievement of open porous structures, also a pycnometric analysis is done. Table 4.1 shows the theoretical- and cylindrical density of 95 % FeS:PES PIP and IPV membranes and 87 %FeS:8 %PVDF:PVDF pills compared to the density obtained by pycnometric analysis. It is expected that by pycnometry only open pore structures can be measured. Therefore pycnometric densities lower than the theoretical density appoints the tested membrane contains encapsulated pores. By dividing these an indication of the fraction of pore space can be given. By doing so the low fraction of -4% for a PIP membrane indicates no encapsulated pores, while for an IPV membrane an encapsulated pore space of 18 % is obtained. For comparison a pressed pill before cycling indicates an increase in density of 18 %, suggesting an increase in density probably due to the applied pressure. Dividing the cylindrical- by the theoretical pore space then gives an indication of total pore space. For a PIP and IPV membrane respectively a pore space of 68 % and 67 % is obtained, while for a pressed pill an unexpectedly high pore space of 47 % is achieved. When including the pycnometric analysis a pore space of 71 % and only 49 % for respectively PIP and IPV membranes is achieved while for pressed pills an unexpected increase in porespace of 65% is obtained due to the increase in density. The lower pore space for IPV- than PIP membranes is in line with the observed smaller surface pore sizes obtained by SEM imagery. The

TABLE 4.1: Density analysis.

<i>Technique</i>	<i>Density (g/cm³)</i>	PIP	IPV	Pressed
Theoretical	■	4,7	4,7	4,4
Pycnometric	■	4,9	3,9	5,2
Cylindric	■	1,5	1,5	2,3
<i>Type</i>	<i>Porespace (%)</i>			
Encapsulated	□	-4,0%	18%	-18%
Total	■	68%	67%	47%
Accessible	■	71%	49%	65%

surprising high amount of pore space for pressed pills in combination with an unexpected increase in density compared to theoretic density could indicate errors during analysis. This is probably due to too low amounts of sample used during Pycnometric analysis. Unfortunately volume determination of the membrane achieved by using gas pycnometric analysis does not clarify ionic adsorption behavior of the surface of membranes and following achievement of ionic conductivity within an aqueous battery. Hence, pursuing this thesis it is advised to do a liquid Mercury- and Brunauer-Emmett-Teller (BET)

surface area analysis in combination with a Barrett-Joyner-Halenda (BJH) pore size and volume analysis considering the occurrence of both big micro- and smaller ultrapores.

4.3 Conclusion

SEM analysis and observations during the process indicate that PES and PVDF membranes successively retain FeS particles, using PIP and IPV production techniques, up to ratios of FeS/polymer = 95:5 %. For PIP membranes containing 25 and 50 % FeS still finger like porous structures are produced. In contrast PIP membranes with 95 % FeS achieve a homogeneous structure

PIP membranes containing 95 % PES with dispersed cross-section micropores in the range of 0.1-15 μm and surface micropores of around 1-1,5 and 0,3-1 μm . IPV laminates also show the achievement of a homogeneous structure with distributed cross-section ultra- and micropores in the range of 0.1-10 μm and surface micropores of respectively 1-6 and 0,5-1 μm . Comparison in the amount of black spots in cross-sections of the laminates indicate a higher total pore volume for the IPV- in comparison to PIP membranes. Density analysis indicate an achievement of pore space of 71%, 49% for respectively PIP and IPV. Pycnometric analysis indicates that the low amount of pore space for IPV membranes is due to the amount of encapsulated pore space. This is in consensus with the obtainment of smaller pore sizes on the surface by using IPV instead of PIP.

Despite the effort, this Chapter gives rather incentives for more extensive research than conclusions. Concise advise for further research is given in the main discussion.

Chapter 5

Cycling performance of PIP and IPV produced FeS anodes

In this chapter PIP and IPV membrane supports carrying FeS, are tested as anode in cycling performance. Figure 5.1 shows a common cycling diagram for NiFeS with its different plateaus indicated. It is assumed plateau's 1 and 2 respectively belong to the Fe/Fe(II) and Fe(II)/Fe(III) couple. Initially membranes consist solely of ferrous iron. From the first cycle onwards an increase can be seen in plateau 2. Several cycles show by manually extending the 1C plateau and following the formation of metallic iron, the capacity of the second plateau subsequently increases. Therefore so-called *Activation cycles*, shown in Figure 5.2 are commonly used for NiFeS batteries to enhance formation of metallic iron, resulting in an increase in electric conductivity, which is not directly proven.[8] Moreover Manohar et al. (2012) suggests that activation cycles have benefiting side-effects. It decreases the surface tension of the electrode surface whereby the electrode gets more wetted resulting in an increase in capacity. Besides, it increases roughening resulting in bigger pore sizes and following an increase in surface area. Thereby the insulating effect of Fe(OH)₂ is suggested to decrease.[42]

The conductivity in an aqueous battery can be separated in ionic- and electronic conductivity. The ionic conductivity is mainly influenced by the accessibility of active surface area and the absorbance of species on the electrode. The electric conductivity is affected by the interconnection of bulk layers and creation or addition of insulating species within the electrode.[8] This thesis introduces a method to enhance the former for NiFeS batteries. On the contrary the latter must not be delimited by doing so; creating too porous structures and using too much insulating additives. Bulk FeS is conductive ranging from 1-5 Ω /cm. IPV membranes contain 95 % FeS show conductivities of 100-1000 Ω /cm. However after cycling Fe(II)(OH)₂ forms by both reactions which is electrically

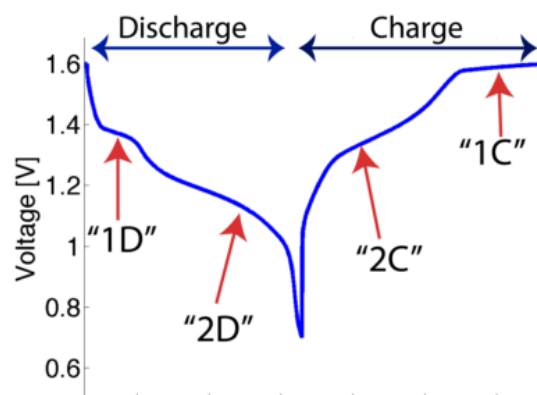


FIGURE 5.1: A typical charge discharge plot of a NiFeS battery with its corresponding plateau's shown, Van Dijk (2012).[8]

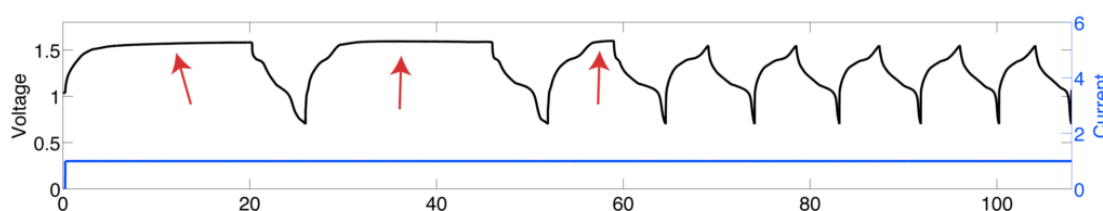


FIGURE 5.2: Activation cycles followed by Fe(II)/Fe(III) cycling, Van Dijk (2012).[8]

insulating. In addition in Chapter 2 it is mentioned both PVDF and PES are electric insulators as well. Hence a conductive additive is favourable to maintain high voltages and rate capacities. A common conductive additive for batteries is amorphous carbon Super P (SP). Commercial NiFe batteries use graphite additives. F. Mulder mentions Ni could be an interesting conductor by adding another feature in inhibiting the HER. Hence also the addition of these conductive additives are tested.

A proposed activation and cycling program by E-Stone Batteries has been used, further explained in the experimental section below. Standard battery tests such as comparing different C-rates and cycling at different temperatures have not been studied as this thesis solely acts as proof of concept. As a benchmark Appendix D shows obtained results by T. van Dijk (2012) for pure pressed FeS pills with capacities of 130 mAh/g for 150 cycles and a cycling efficiency of 82%, solely cycled between assumingly the Fe(II)/Fe(III) couple to prevent the HER.[8]

5.1 Experimental section

For PIP and IPV production specifications of the anodes and ball milling procedures, see the experimental section of Chapter 4. In this report initial mixing, casting of the

polymers, ratio binder in the film and ball milling procedures are considered as fixed parameters.

The used cell set up is custom made by the TUDelft for laboratory use. Two stainless steel flanges press together two circled surfaces of 16 mm, using a spring with within the cell setup. 13 mm anodes are punched out of a film, following 15 mm polycarbonate separators are placed on top. The separator is injected with 50ml 6M KOH (aq) acting as the aqueous electrolyte, which is in the same order of weight as the anode. For the electrolyte KOH pellets are purchased from sigma Aldrich. To make the cell complete a 13 mm Nickel sample is punched out of a cathode of a commercial Toyota Prius NiMH battery. Usually for NiFe batteries, the thicker the separator the lower the self-discharge.[8] Nonetheless, migration of soluble species towards the nickel electrode and influence of separator has not been studied by E-Stone Batteries thus far. If not mentioned otherwise all parameters steps mentioned above have been determined as fixed parameters.

Charge discharge behaviors of cells have been measured via an ARBIN system. A standard program has been applied using 10 activation cycles. During the first five activation cycles a minimum cut off rate of 0,9 V and a maximum cut off rate of 8 hours is used for charging. During the normal cycles a C/5 rate is applied with cut-off maxima of 0,9-1,55 V.

5.2 Results & discussion

5.2.1 PES versus PVDF & PIP versus IPV

Figure 5.3 shows the cycling results for PVDF- and PES membranes containing 95 wt% FeS. Unfortunately miserable discharge rates below 30 mAh/g have been achieved after activation, except for cell 17, having a capacity of 60 mAh/g after 80 cycles. Regarding the theoretical loss in electrolyte volume, due to HER gassing by activation of cells 45-48 low residuals of around 35 ml is common, which is in contrast to cell 17, having 90 ml electrolyte left after activation. Hence a possible explanation could be not enough electrolyte is used for cell 45-48 to survive the activation cycles. As mentioned in Chapter 1, Kitamura et al. (2012) showed that anodes containing PVDF and P(TFE-VDF) turned out to perform a factor 2 worse after 100 cycles than anodes containing PE or PTFE. Therefore the decrease in capacity could also be explained by the use of PVDF as binder.

Considering results between PIP versus IPV membranes no significant differences in performance have been found. This suggests the creation of similar surface layer structures, which is in accordance to the SEM imagery shown in Chapter 5.

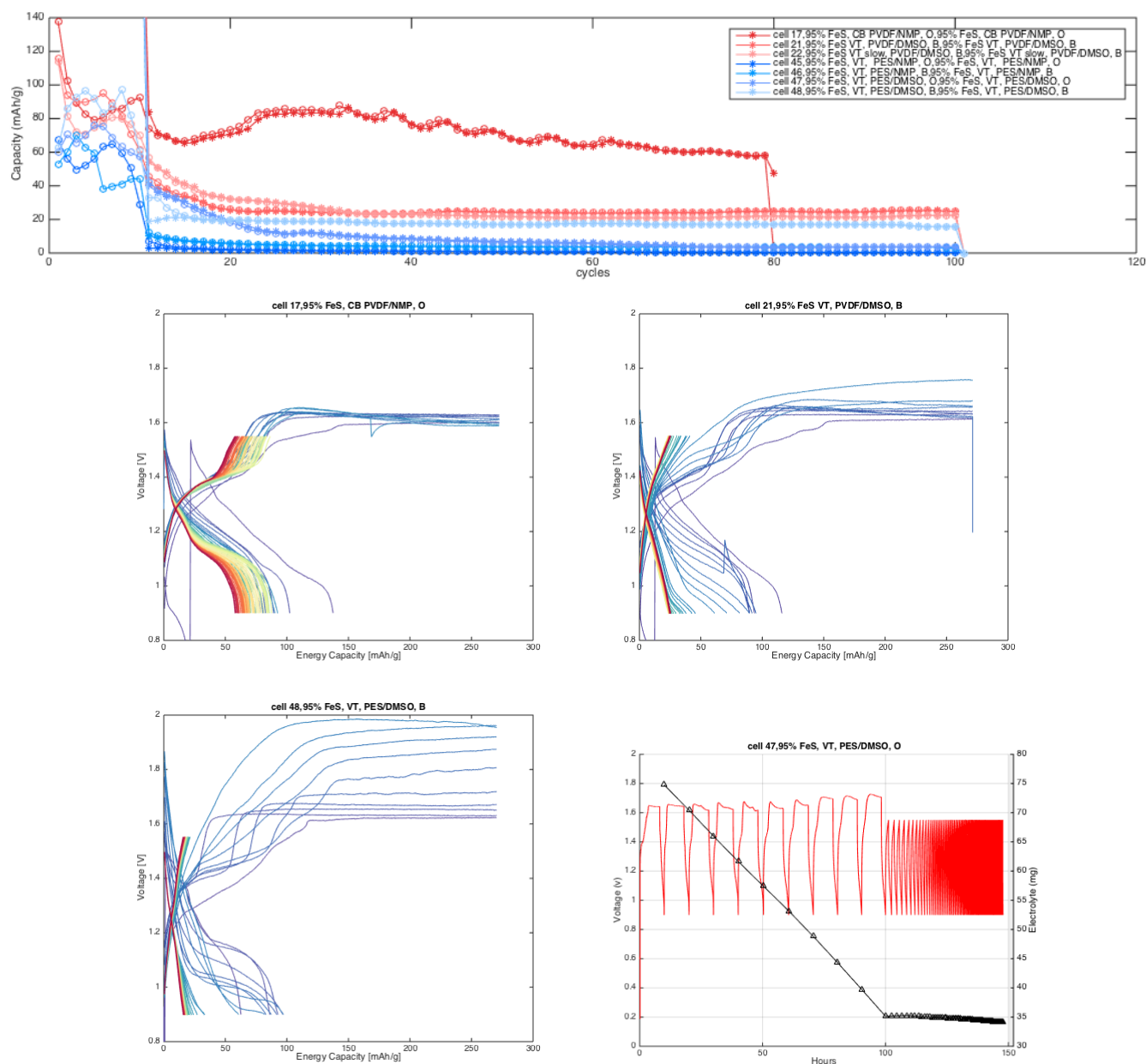


FIGURE 5.3: For FeS/PES versus FeS/PVDF, capacities in mAh/g plotted against the no. of cycles and below for cell 17 and 21 the voltage plotted against the time. Also as an example, for cell 47 the theoretical depletion of electrolyte is shown versus the time. CB means direct PIP and VT means IPV.

5.2.2 PVDF with 15 wt% conductive additive

Figure 5.4 shows cycling results for PVDF membranes using different kinds of 15 wt% conductive additives: Amorphous carbon SP, Graphite or Nickel. During activation promising capacities of 200 mAh/g for SP and 120 mAh/g for Graphite have been achieved. Using nickel shows very deviant voltage cycles, seeming to interfere with the potential of NiFeS. Comparing voltage cycles of 15 wt% to no conductive material suggests additives increase capacity in the activation cycles by at least a factor of 1.5. Below in figure 5.4 for the first normal cycle (11) and cycle 31. graphite and SP are compared to having no conductive additive. For both additives logically a lower over potential is achieved, increasing the capacity. But mostly for SP also a decrease of the plateau in voltage seems to appear, which is favourable for inhibiting the HER.

Despite cycling on only the second plateau, capacity decay occurs for anodes containing SP resulting in 40 mAh/g, while anodes containing Graphite decrease less rapidly to 60 mAh/g after 60 cycles and counting. Regarding electrolyte deficiency; by using lower amounts of FeS per anode in contrast with 95 wt% FeS anodes, theoretical amounts of around 100-150 ml after activation seems to be still sufficient and not to be a limiting factor. Next to the use of PVDF, several other limitations can explain the rapid decrease in capacity as well. For instance the influence of a low overall efficiency. A low efficiency results in irreversible cyclic reactions. For anodes containing graphite the overall efficiency is 1-2 % higher than SP containing anodes. The cycling graphs in figure 5.4 show little HER for anodes containing SP in the initial normal cycles, seeming to explain the lower efficiency. However, compared to the results obtained by T. van Dijk (2012), shown in Appendix D, similar efficiencies of around 80 % have been achieved. Thus it can be concluded lower efficiency does not directly affect the rapid decrease occurring for these batteries. Another plausible explanation is that during activation a rapid built up of metallic iron favours capacity during initial normal cycles. While during further normal cycling an increase in ferrous iron causes the anode to be less conductive. compared to using no conductive additive the capacity decay is occurring less directly. Hence the conductive additives tend to circumvent the electric passivation by the creation of ferrous iron. Concluding, next to the use of PVDF, the most plausible reason for the capacity decrease is the increase in less conductive ferric iron.

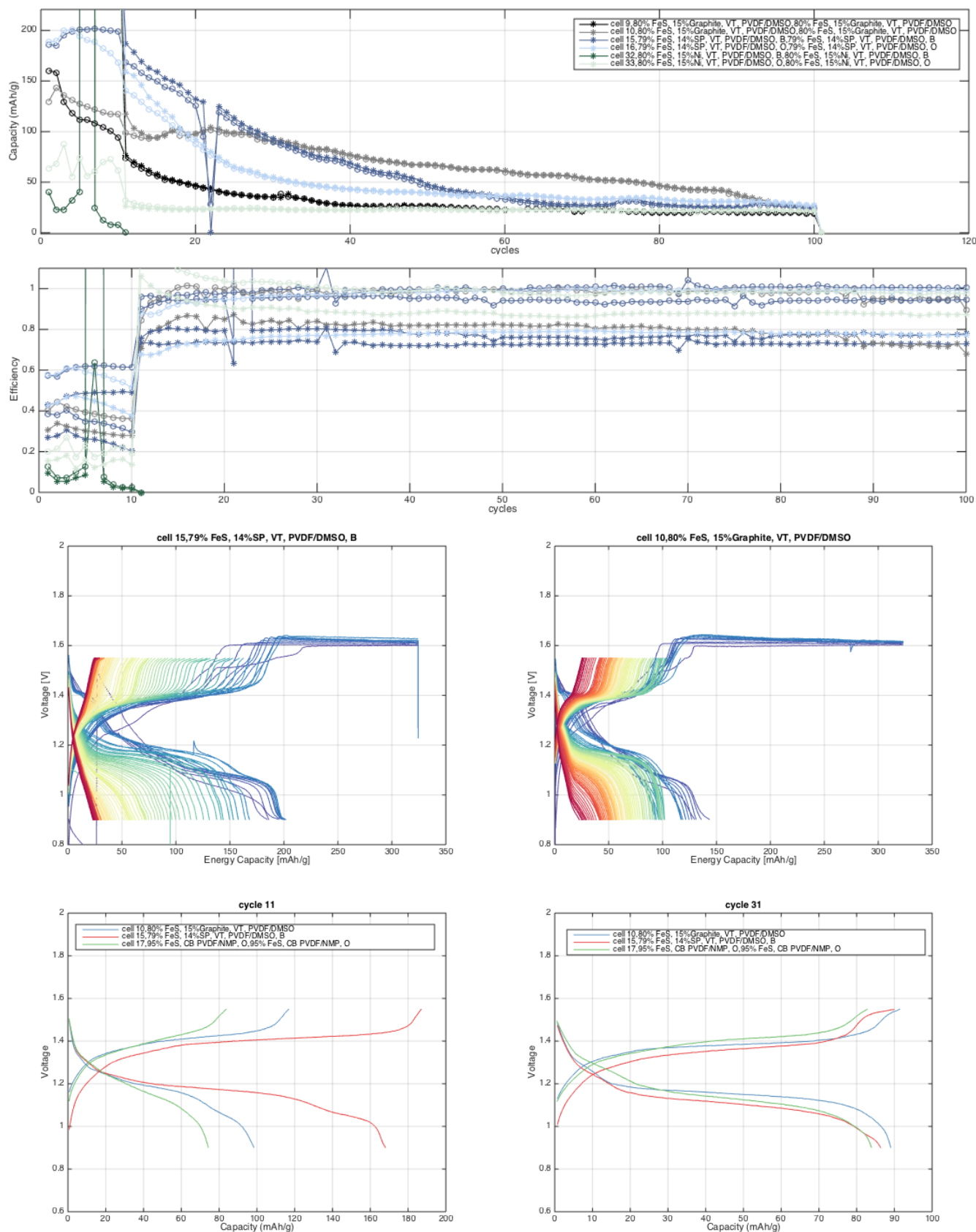


FIGURE 5.4: For FeS/PVDF with 15 wt% conductive additives, capacities in mAh/g and efficiencies plotted against the no. of cycles. below for cell 15 and 10 the voltage is plotted against the time. The progress in cycling is indicated by a color change from blue to red. For cycle 11 and 31 the capacity against the voltage plots are compared for anodes containing Graphite, SP and no additive. VT means IPV.

5.2.3 PVDF with conductive additive super p

An important question is than to what extent does an increase in conductive additive prevent the passivation of the anode? As SP achieved best results compared to graphite and nickel containing anodes, the cycling results of SP containing anodes with different ratios are shown in figure 5.5. Regarding capacity a relation can be found between increase in conductive additive and increase in capacity. However still a very big distribution in capacity can be found for triplo tested anodes, such as 14 wt% SP, indicating reproducibility is still an issue. This could be explained by several factors: The relative poor mixing of the slurries, the clusters formed by ball milling or parameters within the cell other than the anode affect the performance of the battery. The latter would not be surprising considering the big number of parameters playing along.

In the middle of figure 5.5, cycle plots are shown from left to right, for anodes with increasing wt% additive SP. Again it is shown that with decreasing internal electrical resistance, the overpotential decreases. Besides, the voltage plateau's are better defined and much more horizontally flattened, suggesting a better conductivity than when the voltage plateau's are less defined. Hence, more carbon additive increases the energy capacity, indicating conductivity is a limiting factor when FeS is used solely. Also when comparing the cycles of T. van Dijk (2012) for pure pressed pills, shown in Appendix D, the discharge plateau are less defined. Suggesting a conductive additive could be a limiting factor and even higher capacities could have been obtained.

A promising capacity of 180 mAh/g after 55 cycles have been achieved for a pill containing 45 % conducting additive, with overall efficiencies of between 80-82% and coulomb efficiencies between 99-100%, shown in figure 5.5. In contrast to others, this pill remained stable after 50 cycles, until a fatal error occurred of the controlling system. The unrealistic increase in capacity at cycle 25 or 135 hours is probably due to philanthropical interference. Unfortunately reproducibility of the pill seems to be an issue as the slurry is very viscous due to the addition of these lightweight conductive materials with high surface area. Hence considering additives to lower viscosity of the fluid or conductive additives with lower surface area is a suggested alternative. Nickel then qualifies but unfortunately did not attain a happy marriage with FeS.

Moreover, due to a mistake in configuring the cycle program, very high currents have been applied on cells containing high fractions of conductive additive. This accidentally suggests the possibility of NiFeS batteries for application of high performance purposes as well.

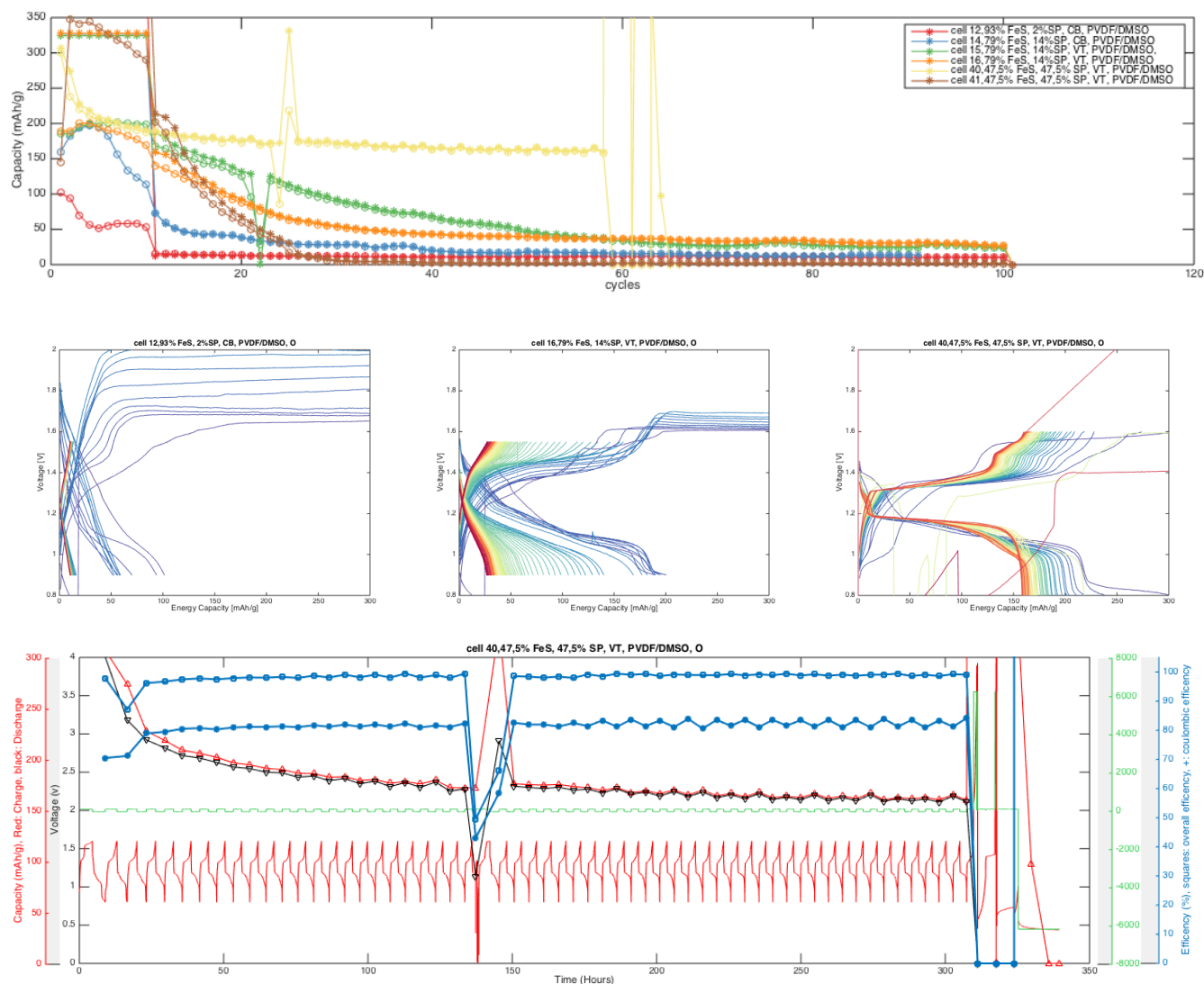


FIGURE 5.5: For FeS/PVDF with increasing SP additive capacities in mAh/g and efficiency plotted against the no. of cycles and below for cell 12 and 16 and 40 the voltage plotted against the time. The progress in cycling is indicated by a color change from blue to red. Also a total voltage plot versus the time for cell 40 is shown below. CB and VT respectively means PIP and IPV.

5.2.4 Ballmilling

Figure 5.6 shows the influence of ball milling on cycling behavior for activation cycle no. 1 and cycle no. 12. By increasing the active surface area it can be seen that the overpotential decreases. Hence by ball milling at least a doubling in capacity is obtained. Assuming bigger FeS particles are more conductive, the decrease of overpotential is mainly caused by an increase in ionic conductivity due to more active surface area per volume. This indicates that enhancement methods to increase ionic conductivity can be measured using this experimental set-up. Nonetheless, the capacities are rather low.

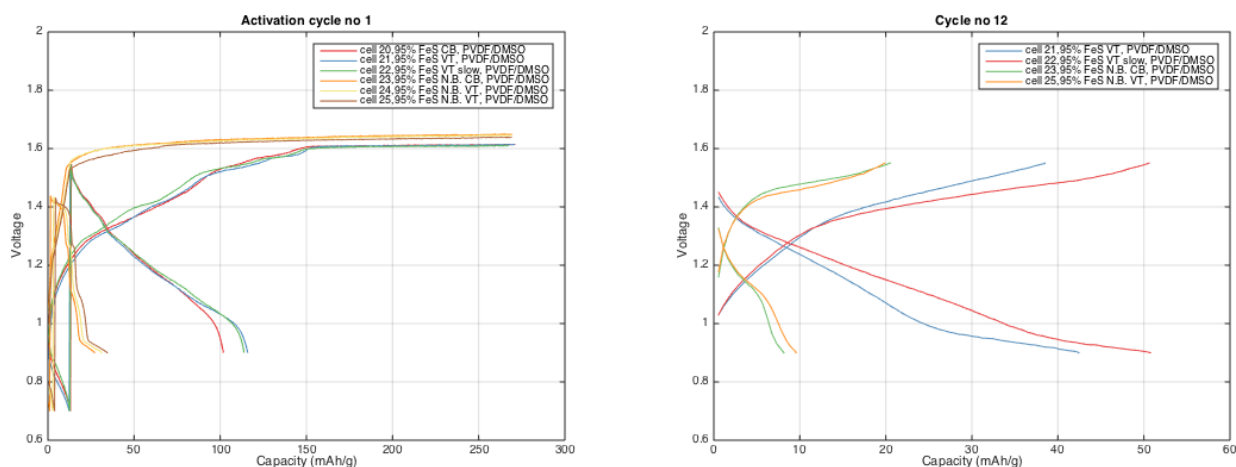


FIGURE 5.6: The voltage plotted against the time for balmilled and not balmilled active material. CB means direct PIP and VT means IPV.

5.3 Conclusion

Multiple achievements of stable electrodes with the most promising result of 180 mAh/g for 55 cycles suggests the implementation of l/l and l/g induced PI techniques to produce thinner and more porous anodes looks promising. However, as a consequence of reproducibility factors and uncertainties considering the set-up, it can not be concluded whether PES nor PVDF containing, PIP nor IPV produced electrodes perform better. Reproducibility of NiFeS is still an issue and not tackled by this polymer study, probably also due to much focus on PI applicable binders. Besides, due to the short cycling results, it is also not proven if the porous structures created by these techniques will sustain in electrochemical conditions. More tests will be needed to investigate what causes reproducibility to be a remaining limiting factor. Therefore it is advised to study l/l and l/g produced anodes in a different experimental set-up that does not apply high pressures on the film, resulting into a more realistic experiment.

Chapter 6

Conclusion

Regarding to what extend is the main question fully answered: *Which kind of polymer-binder fits best in a FeS electrode of a NiFeS battery?* It needs to be concluded that the literature-, and following parameter study done for this thesis is of a too small caliber. This is mainly caused by too much focus on polymers applicable for PIP production techniques.

On the other hand, this thesis has explicitly tried to answer the sub-question: *Is phase immersion precipitation a feasible production technique?* Therefore the literature- and parameter study done in this thesis has been supporting the main question by selecting and deselecting groups of new and common-used synthetic polymers for the application as binder in the FeS electrode of a NiFeS Battery. Most striking is the introduction of the polymer PES and that common used PVDF has been proven not to be resistant for alkaline conditions.

In addition SEM and pycnometry porosity analysis show that PIP produced films do support FeS and an open homogeneous microporous structure can be obtained with cross-section micropore sizes ranging from 0,1-10 μm and surface of respectively 1-6 and 0,5-1 μm with a pore volume of 60%. In comparison surface pore sizes ranging from 0,1-0,5 μm with a pore volume of 50% results by using conventional pressed electrodes. Caution needs to be taken for to highly porous structures and to high amounts of insulating polymer binder as well, as both could negatively affect electronic conductivity.

As a proof of principal, cycling experiments of anodes produced by this novel production method for a Nickel-Iron Sulphide battery show capacities of 180 mAh/g for more than 55 cycles with an average charge/discharge efficiency of 82% can be obtained, by cycling between Fe(II)/Fe(III) only, to prevent the hydrogen evolution.

The achievement of interesting porous structures and increase in porosity compared to conventional production techniques combined with promising cycling results suggest PI by liquid/liquid and gas/liquid demixing techniques could be an interesting production technique.

Chapter 7

Discussion

Yet still several parameters need to be taken into account following the proof of concept. The results obtained in this research use rather basic enhancement techniques and simple mixing methods. It is expected parameters influencing the performance of the electrode, such as active surface area achieved by ball milling procedures, better homogenizing and thinner thickness of the casted slurry can be further enhanced to achieve an increase of cycling performance. Therefore it looks promising to do more extensive cycling tests on parameter enhanced membranes.

A very interesting enhancement parameter to investigate is the hydrophilicity of the obtained anode. Activation cycles are assumed to favour electric- and ionic conductivity by the creation of metallic iron, increase of porosity of the membrane and hydrophilicity. This research introduces the creation of a more porous morphology with the addition of a conductive additive or support. In Chapter 2 the possibility is mentioned to use polymer additives to increase the hydrophilicity. In the perfect case, addition of such a polymer could even eliminate the implementation of activation cycles. A critical note is that hydrophilic polymers decrease chemical- thermal- and mechanical strength of the polymer. As a polymer chain is considered as strong as its weakest link.

This thesis suggests that the main advantages of PIP is the ease of production and the possibility of more porous structures. In the optimal case this is similar to the ideal porous structure of an electrode, mentioned in Chapter 1. Regarding the latter, SEM imagery and pycnometry analysis have not quantitatively defined an increase in pore volume and pore size. Besides, cycling analysis does not clarify symptoms of an increase in ionic conductivity. A liquid mercury- surface area analysis can determine the occurrence of macropores while a BET in combination with a BJH pore size and volume analysis points out the smaller micro and mesopores. In addition, it can indicate a

benchmark of hydrophobicity using adsorption rates. Therefore, pursuing the ambitions of this thesis it is advised to do so.

Besides, it has not been achieved to do actual cycling analysis of such an ideal porous structure, containing sufficient active material. It is very interesting to do more research on performance parameters to acquire this structure and to do actual cycling performance.

Moreover, the endurance over a long lifespan is objected. In this thesis promising cycling behaviour is only achieved for 55 cycles. Considering the cycling behaviour the obtained pores could have the tendency to collapse or fouling can occur within the pores. In comparison life spans of a commercial battery for stationary storage is in the order of 3000 cycles. Hence an analysis of chemical resistance and preservation of porous structures over longer timespans is critical to support the proof of concept.

As already mentioned in Chapter 1 reproducibility of FeS anodes is a common issue. PIP produced anodes have not proven to increase reproducibility of cells. This can suggest the influence of several assumed fixed parameters for this research. Therefore it is advised to question and redetermine cycling test parameters such as the activation cycles, cut off voltages influencing irreversible processes, yet the experimental set-up as well. Research similar to the work of Manohar et al. (2012) could be considered to be of greater value to increase reproducibility of the cell. Manohar et al. examines the influence of different kinds of production techniques and polymers in cycling behaviour for Fe₂O₃ anodes, containing bismuth additives. It is recommended to still do a cycling performance research using different polymers and production techniques but than for FeS, in accordance to the work done by Manohar et al. (2012).

Concerning the research done for this thesis the biggest point of critique concerns the study and examination of enhancement methods, done in Chapter 2 & 3. The attainment of porous structures is studied for pure polymer membranes containing no FeS particles. Nonetheless, as shown by the SEM imagery in Chapter 4, adding particles to the initial solution changes the formation of pores significantly, which is not taken into account by doing so. Hence, it could be interesting to do more literature study to pore morphologies affected by particles. Though, the pore analysis mentioned above in combination with the SEM analysis achieved already gives sufficient funds to be concrete about the actual achievement of a porous structure.

Besides, reassessing the addition of acetone to the solvent DMSO, it has been incorrectly added to the slurries. Acetone has the tendency to evaporate before casting. This decreases the viscosity, which in turn negatively affects the possibility to achieve a cast of the slurry and to add high rates of conductive additive. Hence, it is expected the use

of DMSO favours the achievement of porous structures even more than is observed in Chapter 3. This is also in consensus with the higher solubility parameter of DMSO than NMP.

Appendix A

Polymer synthesis, morphology and properties

A short summary of "The Basic Principles of Membranes" by Jan Mulder (1996): Chapter 2, "Materials and material properties"

Polymer characterization

In short, polymers are macromolecules with high molecular weight, based on repeated units of a basic structure, the monomer. These build up in chains expressed in the degree of polymerization quantifies the number of monomers incorporated in the chain. Thus in principal, the molecular weight depends mostly on the degree of polymerization and logically on the molecular weight of the monomer. As an example the simplest polymer is polyethylene, obtained from ethene, shown below. The resulting character is dependent of the degree of polymerization shown in Table A.1.

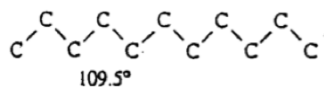
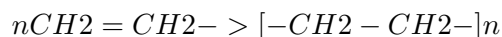


TABLE A.1: relation between molecular weight of a polymer and its resulting character

No. of units of -C ₂ H ₄	Molecular Weight	Character at 25 °C
1	28	Gas
6	170	Liquid
200	5600	Wax
750	21000	Plastic
5000	140000	Plastic

Polyethylene is built up from the same repeated units and is therefore called a homopolymer. Nonetheless the units in a polymer can differentiate. Copolymers are repeating units that differentiate between two monomers. The variation of the monomers in the polymer results in different structures shown in figure A.1a. Also side chains are possible resulting in crosslinking shown in figure A.1b. For example the ability of crosslinking affects the solubility of a polymer.

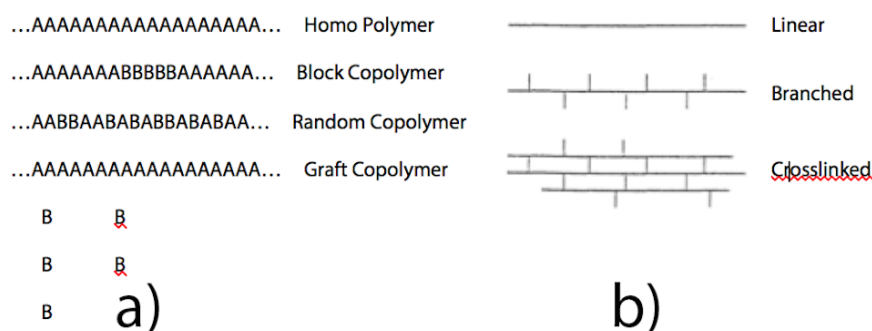


FIGURE A.1: Polymer structuring possibilities

Polymers with side chains are by definition vinyl polymers, characterized by the form $-\text{CH}_2\text{-CHR}-$. Side chains can be attached in three different arrangements shown in figure A.2. In isotactic arrangement all side groups lie on the same side, while in atactic form side chains are arranged randomly along the main chain. Syndiotactic implies the side groups are placed on alternate sides of the main chain.

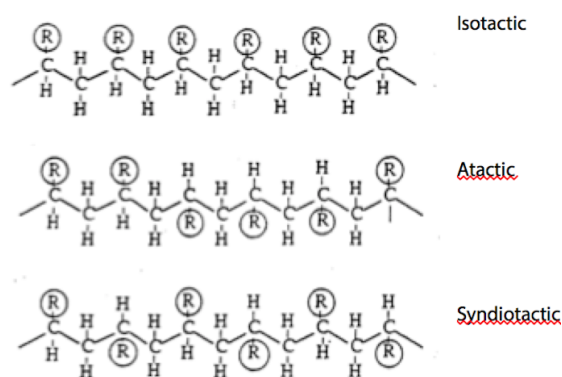


FIGURE A.2: Polymer structuring possibilities

The positioning of the side chains heavily affects the possibility of a polymer to crystallize. Isotactic polymers may be very crystalline while atactic polymers are by definition non-crystalline. Crystallinity in turn affects next to mechanical strength also the permeability of the polymer. When polymers contain a double bond in the main chain it exhibits cis-trans isomerism. Then by polymerization different products can be created with different properties out of one polymer.

Flexibility

A property polymers are known for is flexibility. Most main chains consist solely of -C-C- bonds. Rotation around this bond is possible, which causes the flexible character. Nonetheless a -C=C- bond causes the polymer not to rotate freely and therefore has a very rigid character. Heterocyclic and aromatic groups in the main chain will also cause a significant decrease in flexibility but on the other hand cause chemical and thermal resistant properties. The presence of oxygen and nitrogen in the main chain linked to carbon atom increases flexibility but often aromatic and heterocyclic are present together with oxygen and nitrogen, which causes a rigid character after all. Inorganic polymers also exist not containing carbon atoms in the main chain, such as silicone rubbers and polyphosphazenes. The [-Si-O-] chain is very flexible the [-P=N-] very rigid in turn. Side groups also determine flexibility when the side chain hinders rotation of the main chain. Logically small side chains such as (-H) exhibit smaller hinder in rotational freedom than a phenyl group (-C₆H₅). Bigger side chains also affect inter-chain distance and interaction. figure A.3 shows an overview of flexible and rigid main chains

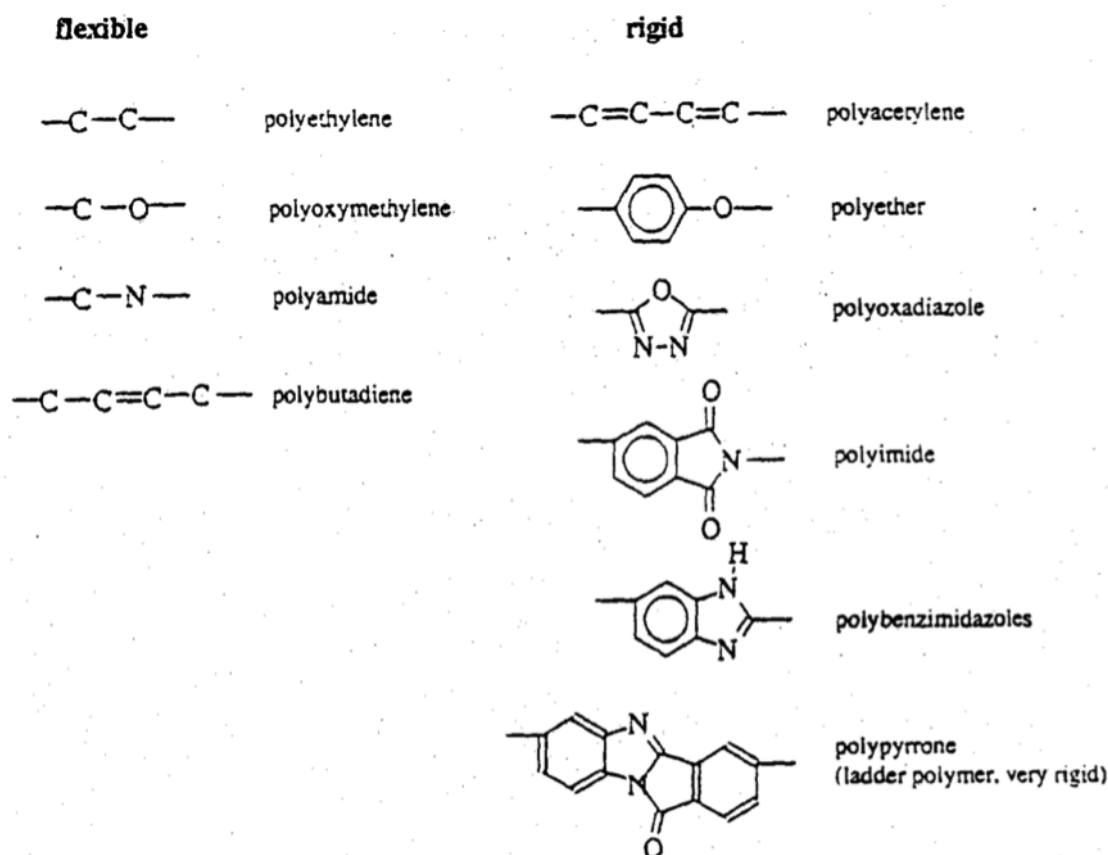


FIGURE A.3: flexible and rigid polymer chains

Moreover, the chain length of the polymer in solution is an important parameter to

determine the average molecular weight. The molecular weight is an important parameter for membrane preparation and characterization. With increasing chain length the number of interaction sites and entanglements between the chains increases shown in figure. Consequently this affects the chemical, physical and mechanical properties of the polymer.

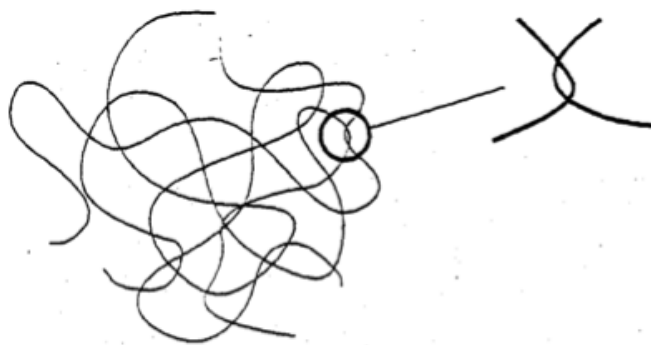


FIGURE A.4: polymer chains with an enlargement of an interaction site

Chain interactions

Actual chain interactions that occur between the chains are for linear and branched polymers only secondary interaction forces. Crystalline polymers have the ability to create primary covalent bonds between chains (400 kJ/mole). These are significantly stronger than secondary interactions. Types of secondary forces that can occur are hydrogen, dipole and dispersion bonding. The strongest secondary force is hydrogen bonding (40 kJ/mole). Hydrogen bonding can be so strong it sometimes can hinder dissolution. This chain interaction occurs when a hydrogen atom attached by an electronegative atom is attracted by an electronegative group of another chain. Strong types of side chains are $-O...H...O-$, $-N...H...O-$ and $-N...H...N-$. Hydrogen bonding can also positively affect crystallization. Table A.2 shows the proton donor and -acceptor character of most common groups. Some polymers can contain groups or atoms of which the charge is not distributed evenly and therefore dipole chain interaction can occur (20 kJ/mole). Some groups with permanent dipoles are hydroxyl ($-OH$), carbonyl ($-C=O$) or halide ($-I$, $-Br$, $-Cl$, or $-F$). Due to fluctuations in electron density dispersion chain interaction can exist (2 kJ/mole). These are the weakest but also the most common forces.

Polymer states

The state of the polymer is defined as the phase in which the polymer appears. State of the polymer is not that important for permeation properties of porous membranes but affects the chemical and thermal properties such that other surface effects as adsorption and wettability are affected (including ionic exchange of the FeS). For amorphous polymers a glassy and rubbery state exists depending on the temperature. The glassy and

TABLE A.2: Proton donor and -acceptor character of most common groups

Group	Proton Donor	Proton acceptor
-OH	X	X
-NH ₂	X	X
-NRH	X	X
-NR ₂		X
-C=O		X
-X (halide)		X
-C ₆ H ₅		X
-C= -N		X

rubbery state are distinguished by difference in tensile strength. The glassy state has a high tensile strength and low volume, while for the rubbery state the tensile strength is much lower and more volume exists. Hence for the rubbery state more freedom exists for the main chains to rotate freely compared to the glassy state. The temperature at which transition from the glassy to the rubbery state occurs is defined as the glass transition temperature (T_g), and is thus considered by chain flexibility and chain interaction. The change in physical behavior by temperature is discontinuous not sudden. Next to volume and strength also other properties change such as specific heat, refractive index, and permeability.

Hence for flexible polymers T_g will be low compared to rigid polymers. Side chains also influence T_g but only when the main chain is considered to be flexible. With increasing size of the chain the T_g increases as well. Logically flexible side groups such as alkyl groups have no effect on the mobility of the main chain, they even decrease T_g due to a decrease in interchain interaction. Next to T_g also crystallinity determines the state of the polymer. By having regular units some polymers are able to crystallize. Per definition atactic polymers are too irregular to crystallize, however other strong intermolecular interactions such as hydrogen bonding can exhibit a semi-crystalline character. Isotactic and syndiotactic polymers generally crystallize. Some polymers can consist of a amorphous and crystalline fraction and are therefore called semicrystalline polymers.

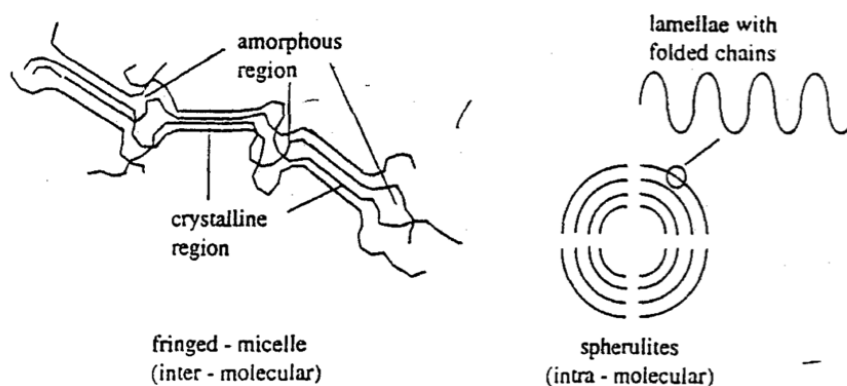


FIGURE A.5: Type of crystallites

The degree of crystallinity provides no information about the size and the shape of the crystallites. Two types of crystallites often found are 'fringed micelles' and 'spherulites'. As can be seen in figure A.5 fringed micelles show sections of adjacent linear polymeric chains in a crystal lattice. Intermolecular ordering occurs. Spherulites occur by slow crystallization of dilute polymer solutions. Crystallization is than intramolecular and occurs in the form of lamellae. Crystallization increases overall mechanical strength. In the rubbery state the tensile strength is reduced until the melting temperature is reached. Hence for crystalline polymers changes occur most at the melting temperature than at the glass transition temperature. Semi-crystalline polymers have the same properties in the glassy state as amorphous polymers but in the rubbery state the mechanical properties are more dependent on the crystal structure of the polymer, shown in figure A.4. Also note the non-existing rubbery state of the polymer for a total crystalline polymer.

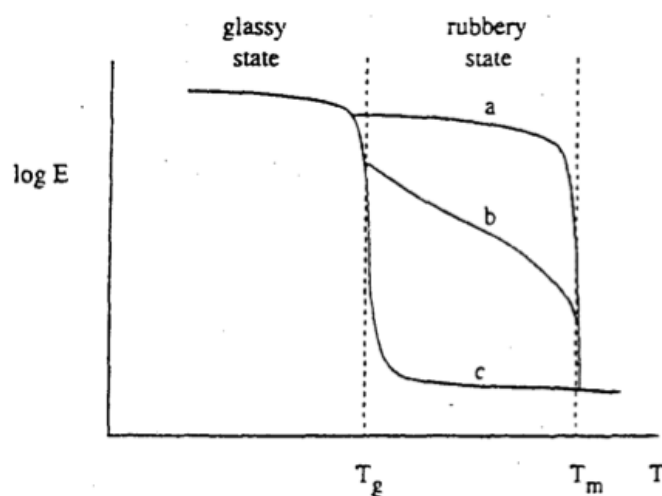


FIGURE A.6: Tensile modulus of a polymer as a function of the temperature. a)crystalline polymer; b)semi-crystalline polymer; c)amorphous polymer.

Next to tensile modulus also the brittleness or toughness is an important parameter. A relatively large force has to be obtained for a glassy polymer whereas for elastomers a small force is sufficient to obtain large deformation. Factors that influence the brittleness are molecular weight, crystallinity and intermolecular forces.

Thus permeability of a polymer heavily depends of the T_g . In general, elastomers (low T_g) show high permeability, glassy polymers on the other hand (high T_g) show low permeability, with some exceptional outliers. T_g also increases by a rigid main chain consisting of aromatic and heterocycling groups without any flexible groups. Crystallinity of a polymer also shows lower permeability. Bulky side groups also increase T_g because of reduction in rotational freedom. Next to permeability, the chemical and thermal stability are also determined by the same structural factors: chain flexibility, chain interactions and crystallinity. Chemical stability is expressed in terms of hydrolytic

stability, solvent resistance, pH- and chlorine resistance. One weak spot such as unsaturated groups, -NH groups, ester groups can already significantly decrease all kinds of resistances. Addition of a diluent can depress the glass transition of a polymer further explained at phase inversion processes.

Mechanical & thermal strength

The definition of chemical and thermal resistance is rather vague and therefore a distinguish should be made between change and loss of properties and decomposition or degradation. The latter often means cleavage of the covalent bond in the main chain and/or side chain. With increasing temperature physical and chemical properties of polymers change and finally degrade. The extent of such change depends on the type of polymer with T_g as an important parameter for amorphous polymers and T_m for crystalline polymers as explained above. Above these temperatures properties change drastically. Parameters that increase thermal and chemical stability are T_g , T_m and crystallinity. Also resonance structures increases thermal stability. But with thermal stability also the production process of the polymer becomes more difficult. Hence process ability and stability oppose each other. Thermoplastic elastomers are a special class of material characterized by the fact that two blocks are not miscible with each other resulting in phase separation. In which one block constitutes the continuous phase and the other block exist as micro-blocks within this continuous phase.

Combining properties

When a homogeneous blend can be created properties of both polymers can be used. Thereby additives can be used in membrane formation. To give desired properties with respect to performance and macrostructure. For example PVP, PAN-f are hydrophilic polymers in contrast with membrane forming polymers such as PI PES PI. Examples are given in figure A.7.

Polymer	T_g (°C)	Blend	T_g (°C)
PEI	217	PEI/PVP	215
PES	225	PES/PVP	201
PI	321	PI/PVP	317
PVP 360,000	177		

FIGURE A.7: Polymer blends

Porous membranes

In contrast with non-porous membranes, the achievement of porous membranes (micro/ultra range) is mainly determined by the processing requirements not by the choice of polymer. Table A.4 shows a classification in type of membrane obtained for different

solvent/non-solvent pairs and table A.4 shows general characteristics of common used microfiltration polymers.

TABLE A.3: Classification of solvent/non-solvent pairs

Solvent	Nonsolvent	Type of membrane
DMSO	water	porous
DMF	water	porous
DMAc	water	porous
NMP	water	porous
DMAc	n-propanol	nonporous
DMAc	i-propanol	nonporous
DMAc	n-butanol	nonporous
trichloroethylene	methanol/ethanol/propanol	nonporous
chloroform	methanol/ethanol/propanol	nonporous
dichloromethane	methanol/ethanol/propanol	nonporous

TABLE A.4: General characteristics of common used microfiltration polymers

Polymer	Structure	flexi- bility	thermo- chemical stabil- ity	Hydro- phobicity	Solvability	Production technique	T _a ,T _m (°C)	Carry FeS
0,1-10 μm								
Polycarbonate	Amorphous	-	++			Grafting, track- etching		
PVDF	Semi- crystalline	+	++	-	+	PI	-40	+
PTFE	Crystalline	+	++	-	-	Sintering, Stretch- ing	126	
PP (isotactic)	Highly crys- talline	+	+	-	-	Sintering, Stretch- ing, PI		
PP (atactic)	Highly crys- talline	+	+	-	-	Sintering, Stretch- ing, PI		
PolyAmide	Amorphous	+	+	+	+	Sintering, track- etching, stretch- ing		
0,001-0,1 μm								
PS	Amorphous	-	+	--	+	PI	190	
PES	Amorphous	-	+	-	+	PI	230	+
PolyEtherImide	Amorphous	-	++	-	+	PI	210	
PolyEtherKetone	Amorphous	-	++		+	PI	143	

Appendix B

200 °C oven treatment

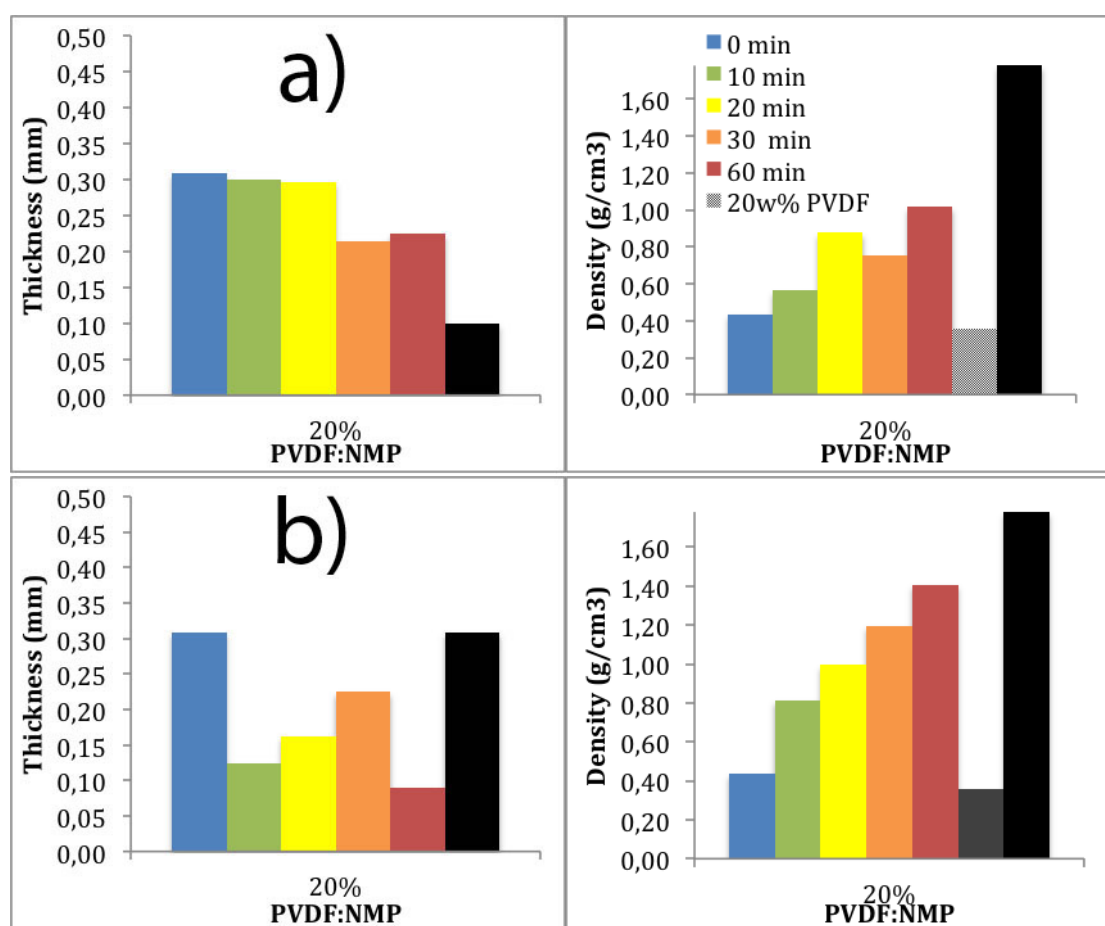


FIGURE B.1: Thickness decrease and density increase due to 200 °C oven treatment of a 0,5 mm casted a) PIP & b) IVP membrane..

Appendix C

SEM photos of FeS, Super P & PVDF particles

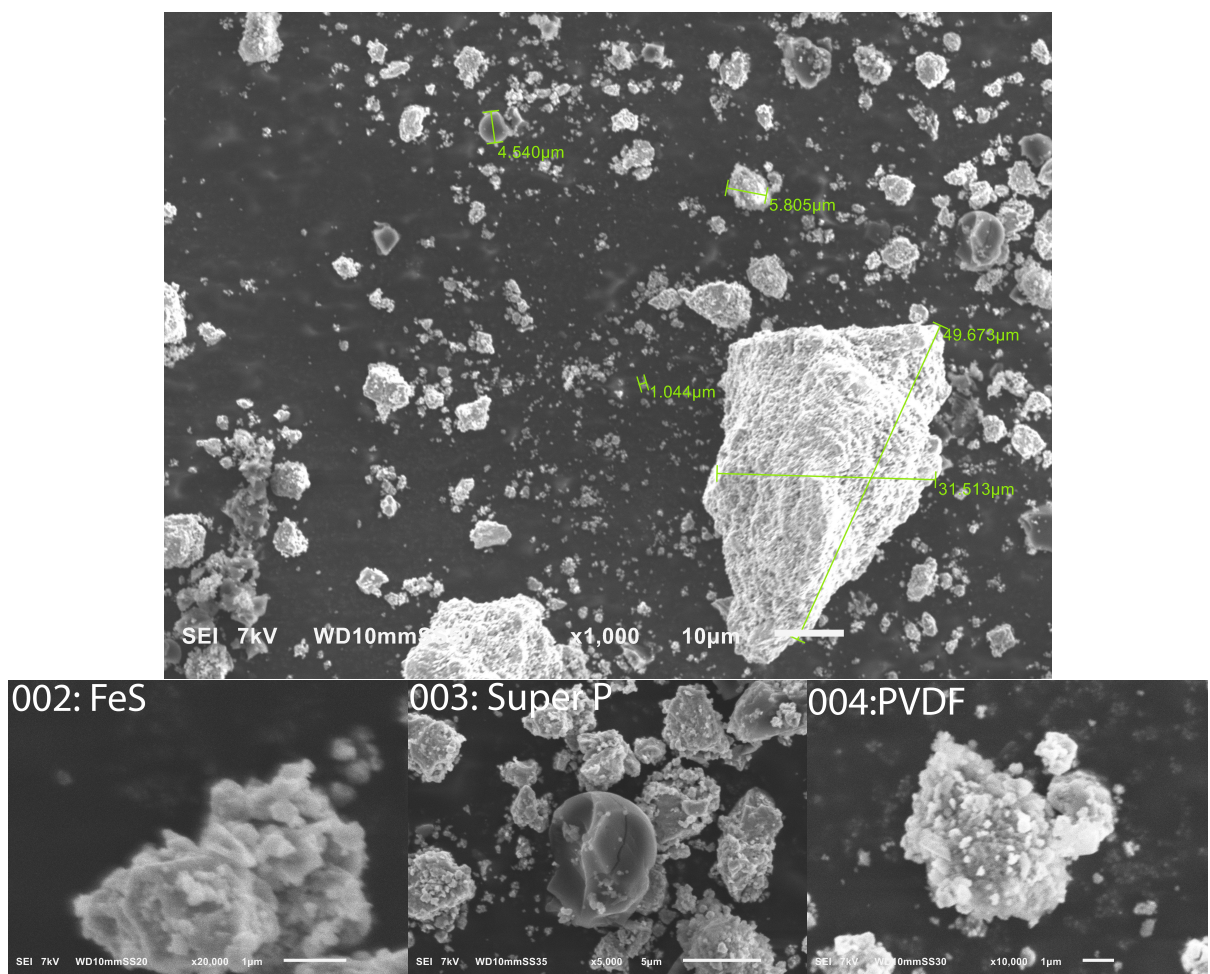


FIGURE C.1: SEM photos of ballmilled FeS, Super P and PVDF

SEM imagery in figure C.1 show ballmilled FeS, blended with Conductive amorphous carbon Super P and binder PVDF particles on carbon tape. the mixture ratio is respectively 82:10:8 wt%. Mapping is used to attain the composition of the overall SEM photo. Then three particles are taken solely to analyze the elementary composition shown in the table on the next page. A wide distribution in sizes can be found with particles of 100 nm to clumps of 50 μm . A distinction can be made between rigid and spherical formations. SEM mapping indicates the spherical shapes are activated amorphous carbon Super P ranging in the μmeter scale. FeS is expected to be globular shaped with hexagonal and monoclinic crystal structures. Due to van der Waals forces ball milled particles smaller than $< \mu\text{m}$ can form aggregates similar to the clumps occurring below.[41] Hence FeS particulates are expected to be much smaller ball milled than seems to appear as the clumps observed on the SEM pictures.

TABLE C.1: Spot elementary Analysis

Chemical formula	w%	atom%	Sigma
Fullpicture			
C	76,26	86,86	0,02
O	11,09	9,48	0,04
S	3,10	1,32	0,01
Fe	9,55	2,34	0,03
Total	100,00	100,00	
002			
C	22,60	48,10	0,03
O	7,95	12,69	0,03
Al*	0,11	0,11	0,01
Si*	0,07	0,06	0,01
S	21,60	17,22	0,02
Fe	47,67	21,82	0,05
Total	100,00	100,00	
003			
C	90,59	93,44	0,01
O	7,53	5,83	0,03
F*	0,52	0,34	0,01
S	0,52	0,20	0,00
Fe	0,84	0,19	0,01
Total	100,00	100,00	
004			
C	74,45	82,77	0,02
O	4,42	3,68	0,03
F	17,88	12,57	0,04
S*	1,12	0,47	0,01
Fe	2,13	0,51	0,01
Total	100,00	100,00	

Appendix D

Results of a pure pressed FeS anode

T. van Dijk (2012): 'A new Nickel-IronSulphide battery, Appendix E'

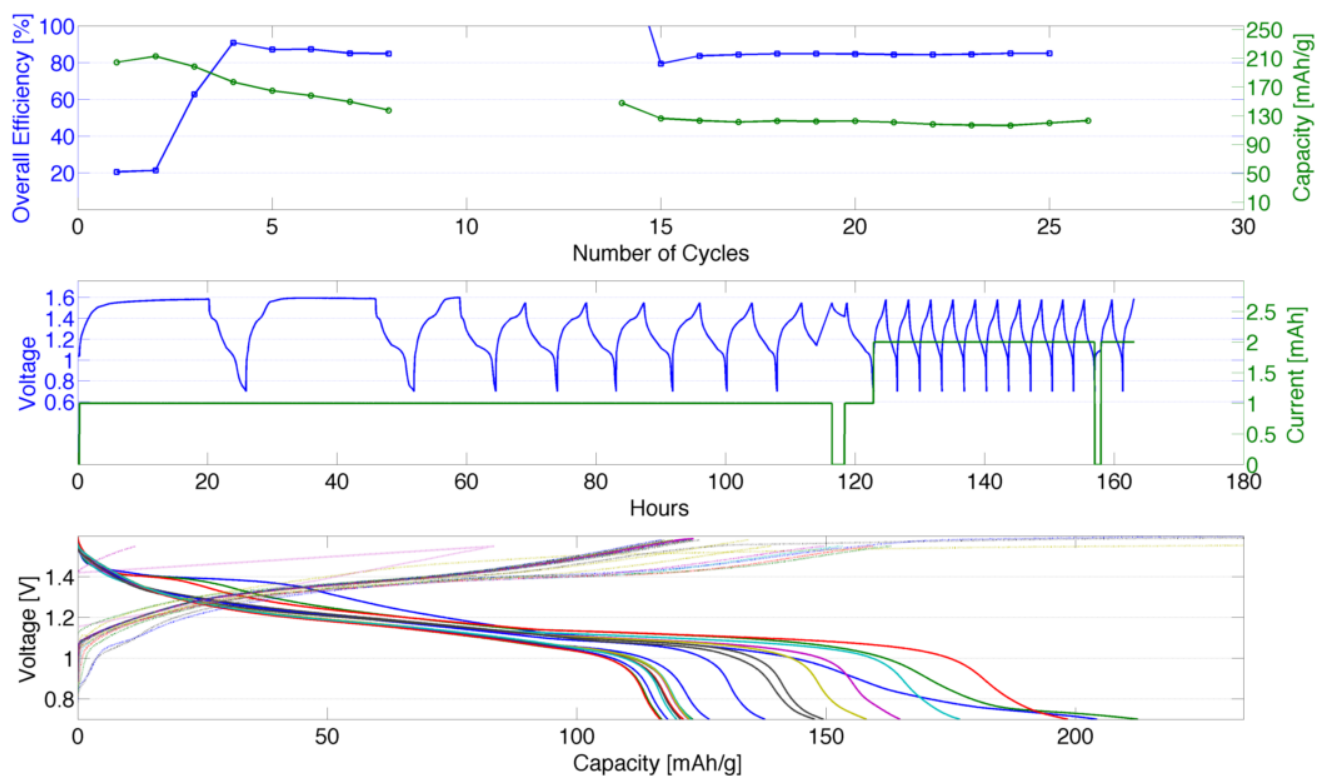


FIGURE D.1: efficiency and capacity plot versus the no. of cycles, voltage plot versus the time and voltage versus capacity

Bibliography

- [1] Thomas van Dijk. E-Stone, STW VG-2 Application, 2014.
- [2] Erik Roesink. *Microfiltration Membrane development and module design*. PhD thesis, University Twente, 1989.
- [3] C. Barth, M.C. Gonçalves, A.T.N. Pires, J. Roeder, and B.A. Wolf. Asymmetric polysulfone and polyethersulfone membranes: effects of thermodynamic conditions during formation on their performance. *Journal of Membrane Science*, 169(2): 287–299, May 2000. ISSN 03767388. doi: 10.1016/S0376-7388(99)00344-0. URL <http://www.sciencedirect.com/science/article/pii/S0376738899003440>.
- [4] Laura Vogelaar, 645–55. doi:10.1002/sml.200400128 Lammertink, Rob G HVogelaar, L., Lammertink, R. G. H., Barsema, J. N., Nijdam, W., Bolhuis-Versteeg, L. A. M., van Rijn, C. J. M., & Wessling, M. (2005). Phase separation micromolding: a new generic approach for microstructuring various materials. *Small* (, Jonathan N Barsema, Wietze Nijdam, Lydia A M Bolhuis-Versteeg, Cees J M van Rijn, and Matthias Wessling. Phase separation micromolding: a new generic approach for microstructuring various materials. *Small (Weinheim an der Bergstrasse, Germany)*, 1(6):645–55, June 2005. ISSN 1613-6829. doi: 10.1002/sml.200400128. URL <http://www.ncbi.nlm.nih.gov/pubmed/17193501>.
- [5] M. Mulder. *Basic Principles of Membrane Technology*. Kluwer Academic Publishers, 1996. ISBN 079234247X.
- [6] Dongliang Wang, K Li, and W.K Teo. Preparation and characterization of polyvinylidene fluoride (PVDF) hollow fiber membranes. *Journal of Membrane Science*, 163(2):211–220, November 1999. ISSN 03767388. doi: 10.1016/S0376-7388(99)00181-7. URL <http://www.sciencedirect.com/science/article/pii/S0376738899001817>.
- [7] Wai-Hung Lau, Micheal Guiver, and T. Matsuura. Phase separation in polysulfone / solvent / water and polyethersulfone / solvent / water systems. *Journal of Membrane Science*, 59:219–227, 1991.

- [8] Thomas van Dijk. *A new Nickel Iron-Sulphide battery*. Thesis, TU Delft, 2012.
- [9] P. van de Witte, P.J. Dijkstra, J.W.a. van den Berg, and J. Feijen. Phase separation processes in polymer solutions in relation to membrane formation. *Journal of Membrane Science*, 117(1-2):1–31, August 1996. ISSN 03767388. doi: 10.1016/0376-7388(96)00088-9. URL <http://linkinghub.elsevier.com/retrieve/pii/0376738896000889>.
- [10] a. K. Manohar, C. Yang, S. Malkhandi, G. K. S. Prakash, and S. R. Narayanan. Enhancing the Performance of the Rechargeable Iron Electrode in Alkaline Batteries with Bismuth Oxide and Iron Sulfide Additives. *Journal of the Electrochemical Society*, 160(11):A2078–A2084, October 2013. ISSN 0013-4651. doi: 10.1149/2.066311jes. URL <http://jes.ecsdl.org/cgi/doi/10.1149/2.066311jes>.
- [11] F. M. Mulder. Implications of diurnal and seasonal variations in renewable energy generation for large scale energy storage. *Journal of Renewable and Sustainable Energy*, 6(3):033105, May 2014. ISSN 1941-7012. doi: 10.1063/1.4874845. URL <http://scitation.aip.org/content/aip/journal/jrse/6/3/10.1063/1.4874845>.
- [12] Nathan S Lewis. Toward cost-effective solar energy use. *Science (New York, N.Y.)*, 315(5813):798–801, February 2007. ISSN 1095-9203. doi: 10.1126/science.1137014. URL <http://www.sciencemag.org.proxy.library.uu.nl/content/315/5813/798.full>.
- [13] Haisheng Chen, Thang Ngoc Cong, Wei Yang, Chunqing Tan, Yongliang Li, and Yulong Ding. Progress in electrical energy storage system: A critical review. *Progress in Natural Science*, 19(3):291–312, March 2009. ISSN 10020071. doi: 10.1016/j.pnsc.2008.07.014. URL <http://www.sciencedirect.com/science/article/pii/S100200710800381X>.
- [14] A.P Karpinski, B Makovetski, S.J Russell, J.R Serenyi, and D.C Williams. Silver-zinc: status of technology and applications. *Journal of Power Sources*, 80(1-2): 53–60, July 1999. ISSN 03787753. doi: 10.1016/S0378-7753(99)00164-0. URL <http://www.sciencedirect.com/science/article/pii/S0378775399001640>.
- [15] A.K. Shukla and B. Hariprakash. *Encyclopedia of Electrochemical Power Sources*. Elsevier, 2009. ISBN 9780444527455. doi: 10.1016/B978-044452745-5.00155-6. URL <http://www.sciencedirect.com/science/article/pii/B9780444527455001556>.
- [16] Atul Sharma, V.V. Tyagi, C.R. Chen, and D. Buddhi. Review on thermal energy storage with phase change materials and applications. *Renewable and Sustainable Energy Reviews*, 13(2):318–345, February 2009. ISSN 13640321. doi: 10.1016/j.

- rser.2007.10.005. URL <http://www.sciencedirect.com/science/article/pii/S1364032107001402>.
- [17] Bruno Scrosati and Jürgen Garche. Lithium batteries: Status, prospects and future. *Journal of Power Sources*, 195(9):2419–2430, May 2010. ISSN 03787753. doi: 10.1016/j.jpowsour.2009.11.048. URL <http://www.sciencedirect.com/science/article/pii/S0378775309020564>.
- [18] E Sosa, R Cabrera-sierra, and Marina E Rinco. Evolution of non-stoichiometric iron sulfide film formed by electrochemical oxidation of carbon steel in alkaline sour environment. *Electrochimica acta*, 47:1197–1208, 2002.
- [19] Bo Yang, Souradip Malkhandi, Aswin K. Manohar, G. K. Surya Prakash, and S. R. Narayanan. Organo-sulfur molecules enable iron-based battery electrodes to meet the challenges of large-scale electrical energy storage. *Energy & Environmental Science*, 7(8):2753, July 2014. ISSN 1754-5692. doi: 10.1039/C4EE01454E. URL <http://xlink.rsc.org/?DOI=C4EE01454E>.
- [20] T. a. Yersak, C. Stoldt, and S.-H. Lee. Electrochemical Evolution of an Iron Sulfide and Sulfur Based Cathode for All-Solid-State Li-Ion Batteries. *Journal of the Electrochemical Society*, 160(8):A1009–A1015, April 2013. ISSN 0013-4651. doi: 10.1149/2.002308jes. URL <http://jes.ecsdl.org/cgi/doi/10.1149/2.002308jes>.
- [21] Jorge Omar Gil Posada and Peter J. Hall. Post-hoc comparisons among iron electrode formulations based on bismuth, bismuth sulphide, iron sulphide, and potassium sulphide under strong alkaline conditions. *Journal of Power Sources*, 268: 810–815, December 2014. ISSN 03787753. doi: 10.1016/j.jpowsour.2014.06.126. URL <http://linkinghub.elsevier.com/retrieve/pii/S0378775314009902>.
- [22] S. M. Abd El Haleem and E. E. Abd El Aal. Electrochemical behaviour of iron in alkaline sulphide solutions. *Corrosion Engineering, Science and Technology*, 43(2):173–178, June 2008. ISSN 1478-422X. doi: 10.1179/174327807X234769. URL <http://www.maneyonline.com/doi/abs/10.1179/174327807X234769>.
- [23] D W Shoesmith, P Taylor, M.G. Bailey, and B Ikeda. Electrochemical Behaviour of iron in alkaline sulphide solutions. *Electrochimica Acta*, 23:903–916, 1977.
- [24] Hiroki Kitamura, Liwei Zhao, Bui Thi Hang, Shigeto Okada, and Jun-ichi Yamaki. Effect of binder materials on cycling performance of Fe₂O₃ electrodes in alkaline solution. *Journal of Power Sources*, 208:391–396, 2012. ISSN 03787753. doi: 10.1016/j.jpowsour.2012.02.051. URL <http://dx.doi.org/10.1016/j.jpowsour.2012.02.051>.

- [25] Chen-Yu Kao and Kan-Sen Chou. Iron/carbon-black composite nanoparticles as an iron electrode material in a paste type rechargeable alkaline battery. *Journal of Power Sources*, 195(8):2399–2404, April 2010. ISSN 03787753. doi: 10.1016/j.jpowsour.2009.08.008. URL <http://linkinghub.elsevier.com/retrieve/pii/S0378775309013238>.
- [26] Shinichi Komaba, Keiji Shimomura, Naoaki Yabuuchi, Tomoaki Ozeki, Hiroharu Yui, and Kohzo Konno. Study on Polymer Binders for High-Capacity SiO Negative Electrode of Li-Ion Batteries. *The Journal of Physical Chemistry C*, 115(27):13487–13495, July 2011. ISSN 1932-7447. doi: 10.1021/jp201691g. URL <http://pubs.acs.org/doi/pdf/10.1021/jp201691g>.
- [27] Sheng Shui Zhang. A review on the separators of liquid electrolyte Li-ion batteries. *Journal of Power Sources*, 164(1):351–364, January 2007. ISSN 03787753. doi: 10.1016/j.jpowsour.2006.10.065. URL <http://www.sciencedirect.com/science/article/pii/S0378775306022452>.
- [28] A. Magistris, P. Mustarelli, F. Parazzoli, E. Quartarone, P. Piaggio, and A. Bottino. Structure, porosity and conductivity of PVdF films for polymer electrolytes. *Journal of Power Sources*, 97-98:657–660, July 2001. ISSN 03787753. doi: 10.1016/S0378-7753(01)00644-9. URL <http://www.sciencedirect.com/science/article/pii/S0378775301006449>.
- [29] A Du Pasquier. Plastic PVDF-HFP electrolyte laminates prepared by a phase-inversion process. *Solid State Ionics*, 135(1-4):249–257, November 2000. ISSN 01672738. doi: 10.1016/S0167-2738(00)00371-4. URL <http://www.sciencedirect.com/science/article/pii/S0167273800003714>.
- [30] Chao Jin, Chenghao Yang, and Fanglin Chen. Effects on microstructure of NiO-YSZ anode support fabricated by phase-inversion method. *Journal of Membrane Science*, 363(1-2):250–255, 2010. ISSN 03767388. doi: 10.1016/j.memsci.2010.07.044. URL <http://dx.doi.org/10.1016/j.memsci.2010.07.044>.
- [31] Ling Zhao, Xiaozhen Zhang, Beibei He, Beibei Liu, and Changrong Xia. Micro-tubular solid oxide fuel cells with graded anodes fabricated with a phase inversion method. *Journal of Power Sources*, 196(3):962–967, February 2011. ISSN 03787753. doi: 10.1016/j.jpowsour.2010.08.074. URL <http://www.sciencedirect.com/science/article/pii/S0378775310014953>.
- [32] Haipeng Zhao, Changyin Jiang, Xiangming He, Jianguo Ren, and Chunrong Wan. Preparation of micro-porous membrane electrodes and their application in preparing anodes of rechargeable lithium batteries. *Journal of Membrane Science*, 310:1–6, 2008. ISSN 03767388. doi: 10.1016/j.memsci.2007.11.044.

- [33] L. Vogelaar, J.N. Barsema, C.J.M. van Rijn, W. Nijdam, and M. Wessling. Phase Separation Micromolding—PS μ M. *Advanced Materials*, 15(16):1385–1389, August 2003. ISSN 0935-9648. doi: 10.1002/adma.200304949. URL <http://doi.wiley.com/10.1002/adma.200304949>.
- [34] Graeme Pearce. Introduction to membranes: Membrane selection. *Filtration and Separation*, 44(April):35–37, 2007. ISSN 00151882. doi: 10.1016/S0015-1882(07)70083-6.
- [35] Shu-lei Chou, Yuede Pan, Jia-zhao Wang, Hua-kun Liu, and Shi-xue Dou. Small things make a big difference: binder effects on the performance of Li and Na batteries. *Physical chemistry chemical physics : PCCP*, 16:20347–20359, 2014. ISSN 1463-9084. doi: 10.1039/c4cp02475c. URL <http://dx.doi.org/10.1039/C4CP02475C> \delimitter"026E30F\$nh<http://www.ncbi.nlm.nih.gov/pubmed/25032670>.
- [36] Munir Cheryan. *Ultrafiltration and Microfiltration Handbook*. CRC Press, 1998. ISBN 1566765986. URL https://books.google.com/books?hl=en&lr=&id=LpiuJVxJS_AC&pgis=1.
- [37] Heru Susanto and Mathias Ulbricht. Characteristics, performance and stability of polyethersulfone ultrafiltration membranes prepared by phase separation method using different macromolecular additives. *Journal of Membrane Science*, 327:125–135, 2009. ISSN 03767388. doi: 10.1016/j.memsci.2008.11.025.
- [38] Zhen-Liang Xu and F Alsahy Qusay. Polyethersulfone (PES) hollow fiber ultrafiltration membranes prepared by PES/non-solvent/NMP solution. *Journal of Membrane Science*, 233(1-2):101–111, April 2004. ISSN 03767388. doi: 10.1016/j.memsci.2004.01.005. URL <http://www.sciencedirect.com/science/article/pii/S0376738804000304>.
- [39] Arkema®. Kynar® & Kynar Flex® PVDF Technical Datasheet. *Performance Characteristics & Data of Thermoplastics for Engineering Applications*, 2009.
- [40] BASF®. Ultrason ® E, S, P Technical Datasheet. Technical report, BASF, 2009.
- [41] Peter Baláz. *Mechanochemistry in Nanoscience and Minerals Engineering*. Springer, Slovakia, 2008. ISBN 9783540748540.
- [42] a. K. Manohar, C. Yang, S. Malkhandi, B. Yang, G. K. Surya Prakash, and S. R. Narayanan. Understanding the Factors Affecting the Formation of Carbonyl Iron Electrodes in Rechargeable Alkaline Iron Batteries. *Journal of the Electrochemical Society*, 159(12):A2148–A2155, 2012. ISSN 0013-4651. doi: 10.1149/2.021301jes.